

Asymptotic Identification Uncertainty of Close Modes

in Bayesian Operational Modal Analysis

Siu-Kui Au¹ and James MW Brownjohn²

Abstract

Close modes are not typical subjects in operational modal analysis (OMA) but they do occur in structures with modes of similar dynamic properties such as tall buildings and towers. Compared to well-separated modes they are much more challenging to identify and results can have significantly higher uncertainty especially in the mode shapes. There are algorithms for identification (ID) and uncertainty calculation but the value itself does not offer any insight on ID uncertainty, which is necessary for its management in ambient test planning. Following a Bayesian approach, this work investigates analytically the ID uncertainty of close modes under asymptotic conditions of long data and high signal-to-noise ratio, which are nevertheless typical in applications. Asymptotic expressions for the Fisher Information Matrix (FIM), whose inverse gives the asymptotic ‘posterior’ (i.e., given data) covariance matrix of modal parameters, are derived explicitly in terms of governing dynamic properties. By investigating analytically the eigenvalue properties of FIM, we show that mode shape uncertainty occurs in two characteristic types of mutually uncorrelated principal directions, one perpendicular (Type 1) and one within the ‘mode shape subspace’ spanned by the mode shapes (Type 2). Uncertainty of Type 1 was found previously in well-separated modes. It is uncorrelated from other modal parameters (e.g., frequency and damping), diminishes with increased data quality and is negligible in applications. Uncertainty of Type 2 is a new discovery unique to close modes. It is potentially correlated with all modal parameters and does not vanish even for noiseless data. It reveals the intrinsic complexity and governs the achievable precision limit of OMA with close modes. Theoretical findings are verified numerically and applied with field data. This work has not reached the ultimate goal of ‘uncertainty laws’, i.e., explicitly relating ID uncertainty to test configuration for understanding and test planning, but the analytical expressions of FIM and understanding about its eigenvalue properties shed light on possibility and provide the pathway to it.

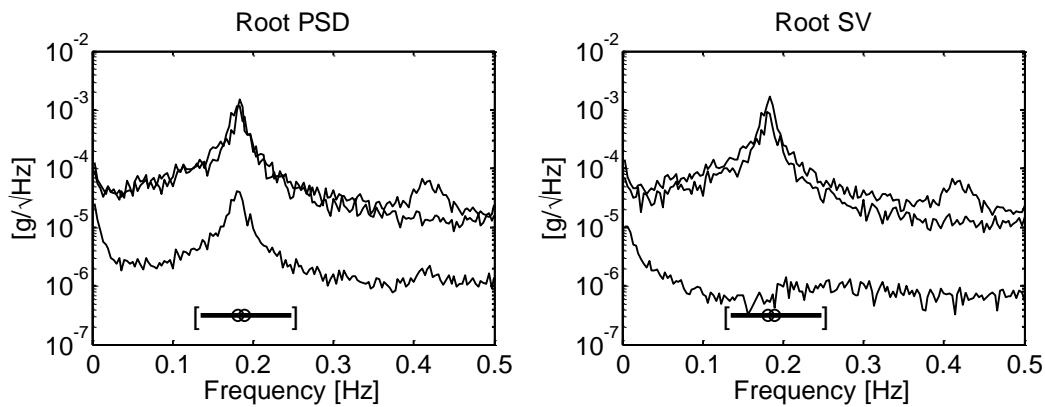
¹ Corresponding author. School of Civil and Environmental Engineering, Nanyang Technological University, 50 Nanyang Avenue, Singapore 639798; E-mail: ivanau@ntu.edu.sg. Formerly with Institute for Risk and Uncertainty and School of Engineering, University of Liverpool, Harrison Hughes Building, Brownlow Hill, Liverpool L69 3GH, UK. E-mail: siukuiau@liverpool.ac.uk

² Centre for Engineering Mathematics and Physical Sciences (CEMPS), University of Exeter, Harrison Building, Exeter EX4 4QF, UK. E-mail: J.Brownjohn@Exeter.ac.uk

27 **Keywords:** ambient modal identification, close modes, Fisher Information Matrix, operational modal
28 analysis, uncertainty laws

29 1 Introduction

30 Modal identification (ID) aims at identifying the in-situ modal properties, e.g., natural frequencies,
31 damping ratios and mode shapes, of a structure based on vibration data [1][2][3]. ‘Well-separated’
32 modes, i.e., a single mode dominating its own resonance band, are typical but ‘close modes’ do
33 occur. The latter are often referred as modes whose natural frequencies are so close that their
34 resonance bands overlap, e.g., visually in the power spectral density (PSD) or singular value (SV, i.e.,
35 eigenvalue of PSD matrix) spectrum of data. Figure 1 gives an example of triaxial ambient
36 acceleration data recorded on a tall building roof. The resonance band indicated by the horizontal
37 bar contains two close modes that are translational in nature.



38
39 **Figure 1 Root PSD and root SV spectrum of triaxial acceleration data on tall building roof. In the**
40 **root PSD plot, the top two lines are x and y, bottom line is z. Bar below peak shows band for**
41 **modal ID**

42 Close modes most typically occur in various forms of tower having two or more horizontal axes of
43 symmetry, e.g., tall buildings [4][5], telecommunication (guyed) masts and freestanding lattice
44 towers [6], cylindrical chimneys [7][8], space launchers [9] and lighthouses [10]. For tall buildings the
45 stiffness and mass properties along two principal directions can be very similar by design, whereas
46 for the other structures symmetry and resultant close modes is a natural consequence of the
47 structural form adopted to fulfil their function against environmental (usually wind) loads.
48 Identifying close modes is important for these structures because they are the effect of subtle
49 differences in stiffness and mass distribution within the almost symmetric structure. Close modes
50 can be found by chance in other structures, such as suspension bridges, e.g., Humber Bridge [11]
51 where closeness of torsional and vertical mode frequencies can affect in-wind dynamics by
52 aeroelasticity.

53 Unlike well-separated modes, close modes are much more challenging in terms of prediction, ID
54 formulation, computational algorithm and ID uncertainty. Theoretically, for modes with identical
55 frequencies, only the subspace spanned by their mode shapes, i.e., 'mode shape subspace' (MSS),
56 rather than the individual ones can be uniquely determined. This is because any linear combination
57 of mode shapes with identical frequencies satisfies the same eigenvalue equation and hence is also a
58 mode shape. Mode shapes with close frequencies have high sensitivity especially within the MSS to
59 perturbations in structural properties [12][13]. A higher order MAC (modal assurance criterion) was
60 defined for close modes in terms of their MSS [14]. The entangling of modal dynamics renders
61 intuition about their behaviour somewhat obscured. In operational modal analysis (OMA) that aims
62 at modal ID based on output-only data, well-separated modes can often be identified with reliable
63 quality from data with reasonable signal-to-noise (s/n) ratio but the same is not true for close modes.
64 Identified mode shapes are inevitably limited to the measured DOFs (degrees of freedom) and so
65 they need not be orthogonal. Many OMA methods only calculate 'operational deflection shapes' for
66 close modes from matrix decomposition (so necessarily orthogonal) rather than the ones in
67 structural dynamics theory. Identifying the mode shapes of close modes requires resolving their
68 coordinates with respect to (w.r.t.) the orthogonal basis spanning their subspace, which are
69 entangled with other modal properties and require sophisticated iterative algorithms, e.g., [15].

70 Significant variability especially in the identified mode shapes can occur from data sets of apparently
71 similar quality. This is often attributed to the sensitivity to underlying properties, e.g., [16] (Section
72 5.3.3) and [17]; but the authors are not aware of any direct account of ID uncertainty. Calculating ID
73 uncertainty for given data is another level of sophistication beyond ID algorithm, for which methods
74 are available depending on the particular modal ID algorithm adopted, e.g., Stochastic Subspace
75 Identification [18][19][20] and Bayesian OMA (BAYOMA) [21][22]. However, the values of the
76 uncertainty bounds do not allow one to understand ID uncertainty and how it depends on the test
77 configuration. The latter aims add to yet another level of challenge that appears intractable,
78 considering the already high sophistication in the ID and uncertainty calculation algorithms; and may
79 not even be possible depending on the intrinsic nature of the problem. Remarkably, recent BAYOMA
80 research on well-separated modes [23] reveals the possibility of insightful asymptotic expressions
81 for the ID uncertainty in terms of test configuration for long data, small damping and high s/n ratio,
82 which are nevertheless typical in applications. Such expressions are collectively referred as
83 'uncertainty laws'.

84 This work takes on the challenge of developing uncertainty laws for close modes. It has not reached
85 the level of insight that has been achieved for well-separated modes but it reports two milestones

86 that are critical to the development and reveal the existence of mathematical beauty. The first
 87 milestone is the high s/n asymptotic expression for the Fisher Information Matrix (FIM) explicitly in
 88 terms of modal properties in the problem; inverting the FIM gives the asymptotic ID uncertainty
 89 (Section 4). The second milestone is the discovery of mutually uncorrelated principal directions of
 90 mode shape uncertainty through analytical study on the eigenvalue properties of the asymptotic FIM,
 91 reducing the complexity of problem so that it does not grow with the number of measured DOFs.
 92 These contributions will be explained qualitatively in Section 2 and technically in Section 5 after
 93 overview of theoretical framework in Sections 3 and 4. Section 6 outlines the theory that establishes
 94 the first milestone with details provided in Sections 13 to 15. Sections 7 and 8 deliver the second
 95 milestone. The theoretical findings are verified and applied in Section 10. The paper is concluded in
 96 Section 11. To facilitate reading, Table 1 lists the abbreviations used in this work.

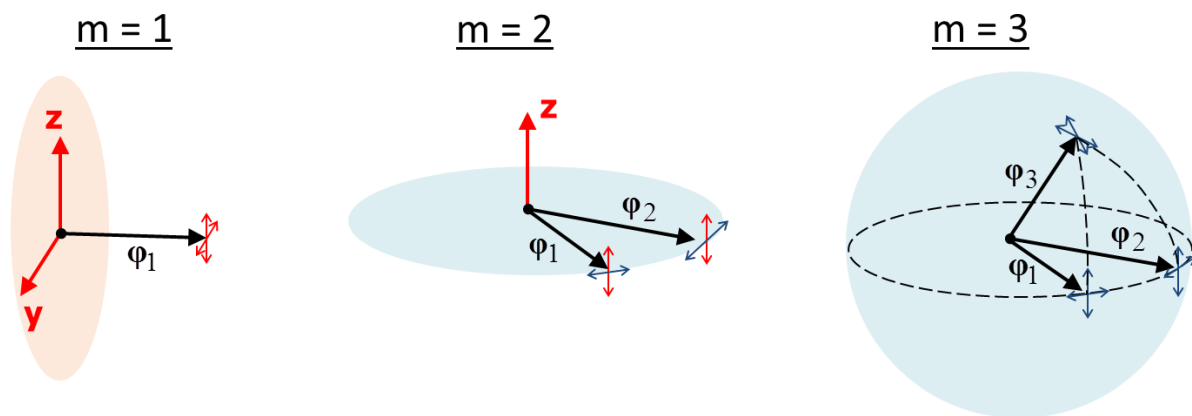
97 **Table 1. Abbreviations used in this work**

Short	Long
BAYOMA	Bayesian Operational Modal Analysis
c.o.v.	Coefficient of variation
DOF	Degree of freedom
FFT	Fast Fourier Transform
FIM	Fisher Information Matrix
i.i.d.	Independent and identically distributed
ID	Identification
MAC	Modal assurance criterion
MPV	Most probable value
MSS	mode shape subspace
OMA	Operational Modal Analysis
PSD	Power spectral density
s/n	signal-to-noise
SV	Singular value
w.r.t.	with respect to

98 **2 Key findings in qualitative terms**

99 To have an appreciation of key discoveries, consider modal ID of m close modes with ambient
 100 triaxial data, i.e., the number of measured DOFs is $n = 3$. The basic assumptions in the ID model (as
 101 in BAYOMA) include linear dynamics with classically damped modes, stationary modal excitations
 102 with constant PSD matrix within resonance band and stationary noise, independent and identically

103 distributed (i.i.d.) among measured DOFs with a constant PSD within the resonance band. Data is
 104 assumed to be sufficiently long in the sense that the number of FFT points in the resonance band is
 105 large compared to 1 (see Section 4); and has high s/n ratio (see (47)). Figure 2 conveys the new
 106 knowledge generated. In each case, the big arrow pointing from the origin (black dot) shows the
 107 mode shape φ_i ; normalised to have unit length. The smaller arrows at the larger arrow tip show
 108 different directions of ID uncertainty. The case of $m = 1$ (well-separated modes) represents what is
 109 currently understood [23]. In this case the uncertainties are all along directions perpendicular to the
 110 mode shape. There are $n - m = 3 - 1 = 2$ such directions, depicted by y and z in the figure; the
 111 plane in red covers all possible directions. There is no uncertainty along the mode shape direction
 112 because the length is constrained to 1. The uncertainties along the y and z direction are uncorrelated.
 113 They are not correlated with other modal properties (e.g., frequency, damping) either. Their size
 114 diminishes with increased data quality and vanishes for noiseless data. In applications it is typically
 115 small and not of concern.



116

117 **Figure 2 Directions of mode shape uncertainty (small arrows at big arrow tip) for $n = 3$ measured**
 118 **DOFs and different number of close modes m . Uncertainty along small red arrows (Type 1) is**
 119 **perpendicular to mode shape subspace (MSS) and vanishes for noiseless data. Uncertainty along**
 120 **small blue arrows (Type 2) is within MSS and prevails even for noiseless data. See also Figure 3.**

121 The cases for $m = 2$ and 3 are close modes, where the new knowledge contributes to. In this case
 122 there are two types of uncertainties, one perpendicular to the mode shapes (Type 1) and the other
 123 within the plane or space they span (Type 2). When $m = 2$, the two mode shapes φ_1 and φ_2 span
 124 over the blue plane (2-D) and there is only one direction (z) perpendicular to it. In addition to the
 125 small red arrow, there is now uncertainty within the blue plane, denoted by the small blue arrow
 126 along the tangential direction of the unit circle. So far recognising these two types of uncertainty
 127 may appear to be mere geometry. The new discovery is that the uncertainties along the two small
 128 red arrows are of a similar nature as their counterpart for $m = 1$, i.e., not correlated with other

129 modal properties and diminish with increased data quality. More remarkable is the uncertainty
 130 along the small blue arrows. It is uncorrelated from the uncertainty of the red arrows but is generally
 131 correlated with all other modal properties. It prevails even for noiseless data and hence represents
 132 the achievable ID precision unique to OMA of close modes. When $m = 3$ the mode shapes span over
 133 a 3-D space and there is no direction perpendicular to all mode shapes (so no red arrows). All
 134 uncertainties are along the small blue directions within the MSS.

135 The above picture is for illustration only. The theory developed in this work applies to general n and
 136 m with no regards to spatial context; and the uncertainties can be quantified with analytical
 137 expressions (see Table 2). It is applicable regardless of how close the modes are. All statements will
 138 be established mathematically in the context of Bayesian inference and asymptotics. Up to
 139 modelling assumptions of classically damped dynamics and stochastic stationary data, the limit on ID
 140 uncertainty is what can be best achieved regardless of the modal ID method adopted, because a
 141 Bayesian approach processes information from data consistent with probability and modelling
 142 assumptions.

143 **3 Bayesian OMA**

144 The Bayesian OMA framework adopted in this work is briefly reviewed here. Consider making
 145 Bayesian inference of the properties of classically damped vibration modes based on (output-only)
 146 ambient vibration data at n DOFs of the subject structure. Without loss of generality, assume that
 147 digital acceleration data $\{\ddot{\mathbf{x}}_j\}_{j=0}^{N-1}$ ($n \times 1$) is measured, from which the ‘scaled’ Fast Fourier
 148 Transform (FFT) can be calculated $\mathcal{F}_k = \sqrt{2\Delta t / N} \sum_{j=0}^{N-1} \ddot{\mathbf{x}}_j e^{-2\pi i j k / N}$, where Δt (sec) is the
 149 sampling interval and k is the FFT index at frequency $f_k = k / N\Delta t$ (Hz). The FFT (the sum) has been
 150 scaled by $\sqrt{2\Delta t / N}$ so that the expectation $E[\mathcal{F}_k \mathcal{F}_k^*]$ (** denotes complex conjugate transpose)
 151 gives the one-sided PSD matrix of data. Only the scaled FFT within a selected resonance band
 152 covering the modes of interest is used for modal ID, which is found to play a balance between ID
 153 precision (information from bands off resonance is negligible) and modelling error (ID results are
 154 immune to activities outside resonance band) .

155 Within the resonance band the scaled FFT of data is modelled as $\mathcal{F}_k = \sum_{i=1}^m \boldsymbol{\varphi}_i \ddot{\eta}_{ik} + \boldsymbol{\xi}_k$ where m is
 156 the number of modes; $\boldsymbol{\xi}_k$ ($n \times 1$) is a vector of data noise, assumed to be i.i.d. among different DOFs
 157 with a common PSD S_e within the resonance band (so only band-limited white); $\boldsymbol{\varphi}_i$ ($n \times 1$) is the

158 mode shape, real-valued because the mode is assumed to be classically damped; $\dot{\eta}_{ik}$ (scalar) is the
159 scaled FFT of modal acceleration response, whose time-domain counterpart satisfies (omitting
160 dependence on time) $\ddot{\eta}_i + 2\zeta_i\omega_i\dot{\eta}_i + \omega_i^2\eta_i = p_i$; $\omega_i = 2\pi f_i$ (rad/sec) and f_i is the natural
161 frequency (Hz), ζ_i is the damping ratio, p_i is the modal force (per unit modal mass). Strictly
162 speaking, the noise PSDs at different DOFs are never the same because no two data channels are
163 identical. The BAYOMA framework so far has assumed a common noise PSD as it is found to
164 significantly simplify mathematics, allowing development of fast algorithms for posterior statistics.
165 Experience reveals that the ID results (both most probable value and ID uncertainty) of other modal
166 parameters (the main interest) are insensitive to violation of this assumption unless the s/n ratio is
167 low and the noise PSDs differ by several orders of magnitude. This is also consistent with the
168 uncertainty law for well-separated modes where for high s/n ratios the noise PSD is asymptotically
169 uncorrelated from the remaining parameters [23]. The modal forces $\{p_i\}_{i=1}^m$ are assumed to be
170 stochastic stationary with a constant PSD matrix \mathbf{S} ($m \times m$ Hermitian and positive definite) within
171 the resonance band (so only band-limited white). The modal properties to be identified comprise
172 $\{f_i\}_{i=1}^m$, $\{\zeta_i\}_{i=1}^m$, \mathbf{S} , S_e and $\Phi = [\phi_1, \dots, \phi_m]$. Accounting for its Hermitian nature, \mathbf{S} has m^2
173 parameters: m for the real diagonal entries and $m(m-1)$ for the complex-valued lower off-
174 diagonal entries. In total there are $m + m + m^2 + 1 + mn = (m+1)^2 + mn$ parameters, subjected to
175 m unit norm constraints on the mode shapes.

176 Given the scaled FFT as data, the ID results are encapsulated in the ‘posterior’ (i.e., given data) PDF
177 (probability density function) of modal parameters, which is proportional to the product of the
178 likelihood function and prior PDF. Assuming long data, the scaled FFT can be shown to follow a
179 (circularly symmetric) complex Gaussian PDF. The likelihood function is then equal to $\exp(-L)$
180 where $L = nN_f \ln \pi + \sum \ln |\mathbf{E}_k| + \sum \mathcal{F}_k^* \mathbf{E}_k^{-1} \mathcal{F}_k$ is the negative log-likelihood function; $|\cdot|$ denotes
181 the matrix determinant; the sums without index are over all k in the resonance band for modal ID
182 (same notation throughout this work);

$$183 \quad \mathbf{E}_k = \overline{\Phi} \mathbf{H}_k \overline{\Phi}^T + S_e \mathbf{I}_n \quad (1)$$

184 is the theoretical PSD matrix of data that depends on the modal parameters; \mathbf{I}_n is the $n \times n$ identity
185 matrix;

$$\bar{\Phi} = [\bar{\Phi}_1, \dots, \bar{\Phi}_m] \quad \bar{\Phi}_i = \Phi_i / \|\Phi_i\| \quad \|\Phi_i\|^2 = \Phi_i^T \Phi_i \quad (2)$$

186 is the normalised mode shape matrix; \mathbf{H}_k is the theoretical $m \times m$ PSD matrix of modal response
 187 whose (i, j) -entry is $S_{ij} h_{ik} h_{jk}^*$ where $h_{ik} = 1 / [(1 - \beta_{ik}^2) - \mathbf{i}(2\zeta_i \beta_{ik})]$ is the frequency response
 188 function between the modal force p_i and modal acceleration $\ddot{\eta}_i$; $\beta_{ik} = f_i / f_k$. Leakage has been
 189 neglected in (1) as it is asymptotically small when the data duration is long (in the sense $N_f \gg 1$,
 190 see Section 4), which is assumed in the study of uncertainty laws and holds in typical cases where
 191 the ID uncertainty is under control. Empirically, a value of N_f in the order of a few tens (e.g., 30)
 192 may be considered sufficiently large for this purpose. In situations when leakage is significant there
 193 will be modelling error which is not accounted by the present study or existing uncertainty laws. See
 194 Section 10.2.6 of [18] for a discussion of this issue.

196 OMA data is often sufficiently long that prior information is irrelevant and hence the prior PDF is
 197 assumed to be uniform. The posterior PDF is then directly proportional to the likelihood function. It
 198 can be well-approximated by a Gaussian PDF (w.r.t. modal parameters). The mean, or equivalently
 199 ‘most probable value’ (MPV) of the posterior PDF maximises the likelihood function, or equivalently
 200 minimises the negative log-likelihood function. The covariance matrix of the Gaussian PDF, i.e.,
 201 ‘posterior covariance matrix’, is equal to the inverse of the Hessian of the negative log-likelihood
 202 function at the MPV. An efficient algorithm (referred as BAYOMA) applicable for multiple (possibly
 203 close) modes has been developed which allows Bayesian OMA to be performed typically in a matter
 204 of seconds; see [22] for original work and Chapter 13 of [21] in consolidated form. See [24]-[27] for
 205 some recent applications.

206 **4 Long data asymptotics**

207 The Bayesian approach in the last section allows one to calculate the ID uncertainty of modal
 208 properties for a given data set but it does not offer any insight on how it depends on the test
 209 configuration or environment. One way to do that is to introduce a ‘frequentist’ assumption that the
 210 data indeed corresponds to some ‘true’ modal properties and study the behaviour of the posterior
 211 covariance matrix under some asymptotic yet realistic conditions such as long data and high s/n
 212 ratio. The resulting expressions are collectively referred as ‘uncertainty laws’. For globally
 213 identifiable problems such as OMA, it has been found that the asymptotic behaviour of the posterior
 214 covariance matrix is intimately related to the Fisher Information Matrix (FIM) [28]. For long data
 215 ($N_f \gg 1$) the leading order of the posterior covariance matrix \mathbf{C} is equal to the inverse of the FIM,

216 i.e., $\mathbf{C} = \mathbf{J}^{-1}[\mathbf{I} + O(1/\sqrt{N_f})]$, where \mathbf{I} denotes the identity matrix, $O(1/\sqrt{N_f})$ is the remainder
 217 that depends on data and is of the order of $1/\sqrt{N_f}$; N_f is the number of FFT points in the
 218 selected band, equal to the product of bandwidth and data duration. The matrix \mathbf{J} is the FIM, equal
 219 to the expectation of the Hessian of negative log-likelihood function evaluated at the ‘true’
 220 parameter values and assuming that the scaled FFT data is indeed distributed as the likelihood
 221 function. As the scaled FFT is complex Gaussian, it follows from a standard result in multivariate
 222 statistics [29] that the entry of FIM corresponding to generic parameters x and y is given by

$$223 \quad J_{xy} = \text{tr} \Sigma[\mathbf{E}_k^{-1} \mathbf{E}_k^{(x)} \mathbf{E}_k^{-1} \mathbf{E}_k^{(y)}] \quad (3)$$

224 where $\text{tr}(\cdot)$ denotes the trace of a square matrix, i.e., sum of diagonal entries; the superscript ‘ (x) ’
 225 denotes a derivative w.r.t. x . On the other hand, it should be noted that, with some abuse of
 226 notation, in the FIM, the parameter symbols in the expression represent the ‘true’ value of
 227 properties rather than the dummy variable in Bayesian inference. That is, the FIM is a function of the
 228 true parameter values and not the data (which has already been averaged in the expectation).

229 It should be noted that the ID uncertainty in this work (as in BAYOMA) refers to that implied by the
 230 posterior PDF of modal parameters in a Bayesian context. The connection with frequentist concept
 231 lies only in the additional assumption that the data indeed follows a distribution for some ‘true
 232 values’ of modal parameters. This assumption is introduced only for the study of uncertainty laws (to
 233 understand uncertainty). It is not involved in the modal identification process where uncertainty for
 234 a given data set is calculated (but whose value provides no understanding). Detailed discussion of
 235 the meaning and interpretation of uncertainty in Bayesian and frequentist sense can be found in [28]
 236 and Section 9.6 of [21].

237 **5 Key theoretical findings**

238 Developing insights into ID uncertainty requires analytical investigation of FIM and its inverse to give
 239 the asymptotic posterior covariance matrix as the uncertainty law, if possible, in the form of explicit
 240 closed form expressions that link with test configuration and environment. This has been
 241 accomplished for well-separated modes but turns out to be very challenging for close modes. As the
 242 first key contribution of this work, we obtained asymptotic expressions for the FIM for high s/n ratio
 243 ($S_e \rightarrow 0$). The results are summarised in Table 2. When $m = 1$, it gives the same expressions for

244 well-separated modes that have been previously obtained; see Table 16.1 in Section 16.1.1 of [21].

245 In Table 2,

$$246 \quad \mathbf{Q} = \mathbf{I}_n - \overline{\Phi}(\overline{\Phi}^T \overline{\Phi})^{-1} \overline{\Phi}^T \quad (4)$$

$$247 \quad \mathbf{Q}_i = (\overline{\Phi}^T \overline{\Phi})^{-1} \overline{\Phi}^T (\mathbf{I}_n - \overline{\Phi}_i \overline{\Phi}_i^T) \quad [\mathbf{Q}_i] = \begin{bmatrix} \mathbf{Q}_1 & & \\ & \ddots & \\ & & \mathbf{Q}_m \end{bmatrix} \quad (5)$$

$m \times n$ $m^2 \times mn$

248 \mathbf{e}_i is a $m \times 1$ zero vector except for the i th entry equal to 1; $[\mathbf{e}_j \mathbf{e}_i^T]$ denotes a $m^2 \times m^2$ matrix

249 whose (i, j) -partition is $\mathbf{e}_j \mathbf{e}_i^T$; Φ : is the 'vectorisation' of Φ , i.e., a $mn \times 1$ vector obtained by

250 stacking the columns of Φ column-wise. In the derivation, it has been assumed that the mode

251 shapes are linearly independent (but not necessarily orthogonal) and modal forces are not perfectly

252 coherent (i.e., \mathbf{S} non-singular), for otherwise the modal ID problem degenerates. The derivation will

253 be outlined in Section 6 with details postponed to Section 13 (appendix) for J_{xy} ($x, y = \{f, \zeta, \mathbf{S}\}$),

254 J_{xS_e} and $J_{S_e S_e}$; and to Section 14 and 15 (appendices) for $J_{x\Phi_i}$, $J_{S_e \Phi_i}$ and $J_{\Phi:\Phi}$. Their

255 asymptotic correctness will be verified in Section 10.1.

256 As the second (but no less important) key contribution of this work, based on Table 2, we investigate

257 analytically the eigenvalue properties of $\mathbf{J}_{\Phi:\Phi}$, the full FIM \mathbf{J} (i.e., comprising all parameters) and

258 hence the high s/n asymptotic posterior covariance matrix. We found that the eigenvectors of the

259 full FIM, and hence the asymptotic covariance matrix, comprise three types induced by those of

260 $\mathbf{J}_{\Phi:\Phi}$ that carry independent and distinctive influence on ID uncertainty. They are summarised in

261 Table 3; the definitions of \mathcal{N} , \mathcal{M} and \mathcal{M}_\perp in the table will become apparent in Section 7.

262 Theoretical details can be found in Section 8. The theoretical findings will be illustrated in Section 10

263 using synthetic and field data.

264 As a remark, for well-separated modes a fundamental definition of s/n ratio that directly affects ID

265 uncertainty is the PSD ratio of modal response to noise at the natural frequency [23]. In this case

266 high s/n ratio refers to the case when this ratio is large compared to 1. For close modes the present

267 work has not yet concluded a fundamental definition for s/n ratio with the same success mentioned

268 above. The condition $S_e \rightarrow 0$ was given earlier as a simple limit condition to qualify for the

269 theoretical results. See also (47) that is a dimensionless but more involved condition that can

270 potentially lead to a definition in the future useful for quantifying ID uncertainty for close modes.

271 When applying the asymptotic results for cases with clearly different channel noise PSDs, one may
272 use a value of S_e with a representative order of magnitude, e.g., the geometric mean of channel
273 noise PSDs.

274 **Table 2 Asymptotic expressions for FIM for high s/n ratio. ‘ $x, y = f, \zeta, \mathbf{S}$ ’ denotes that x and y are frequency, damping or real/imaginary part of**
 275 **auto/cross PSDs, i.e., those affecting the PSD matrix of modal response \mathbf{H}_k . See (4) for \mathbf{Q} and (5) for \mathbf{Q}_i ; \mathbf{e}_i and Φ : are explained thereafter; $[\mathbf{Q}_i]$**
 276 **denotes a block diagonal matrix containing the \mathbf{Q}_i s and $[\mathbf{e}_j \mathbf{e}_i^T]$ denotes a $m^2 \times m^2$ matrix whose (i, j) -partition is $\mathbf{e}_j \mathbf{e}_i^T$.**

	$x, y = f, \zeta, \mathbf{S}$	S_e	Φ_1, \dots, Φ_m
$x, y = f, \zeta, \mathbf{S}$	$J_{xy} \sim \text{tr} \Sigma [\mathbf{H}_k^{-1} \mathbf{H}_k^{(x)} \mathbf{H}_k^{-1} \mathbf{H}_k^{(y)}]$	$J_{xS_e} \sim \text{tr} [(\overline{\Phi}^T \overline{\Phi})^{-1} \Sigma \mathbf{H}_k^{-1} \mathbf{H}_k^{(x)} \mathbf{H}_k^{-1}]$	$J_{x\Phi_i} \sim 2\mathbf{e}_i^T (\text{Re} \Sigma \mathbf{H}_k^{(x)} \mathbf{H}_k^{-1}) \mathbf{Q}_i$ $1 \times mn$
S_e		$J_{S_e S_e} \sim N_f (n-m) S_e^{-2}$	$J_{S_e \Phi_i} \sim 2\mathbf{e}_i^T (\overline{\Phi}^T \overline{\Phi})^{-1} (\text{Re} \Sigma \mathbf{H}_k^{-1}) \mathbf{Q}_i$ $1 \times mn$
Φ_1, \dots, Φ_m	Symmetric		$J_{\Phi:\Phi} \sim J_{\Phi:\Phi}^{(1)} + J_{\Phi:\Phi}^{(2)}$ $mn \times mn$ $J_{\Phi:\Phi}^{(1)} = 2S_e^{-1} (\text{Re} \Sigma \mathbf{H}_k) \otimes \mathbf{Q}$ $J_{\Phi:\Phi}^{(2)} = 2[\mathbf{Q}_i]^T \left\{ (\text{Re} \Sigma \mathbf{H}_k \otimes \mathbf{H}_k^{-T}) + N_f [\mathbf{e}_j \mathbf{e}_i^T] \right\} [\mathbf{Q}_i]$

277 **Table 3 Eigenvalue properties of full FIM \mathbf{J} ; MSS = mode shape subspace; assume mode shapes**
 278 **$\{\boldsymbol{\varphi}_1, \dots, \boldsymbol{\varphi}_m\}$ appear in the last mn entries of the full set of modal parameters; see Table 4 for**
 279 **definitions of \mathcal{N} , \mathcal{M} and \mathcal{M}_\perp**

Type	Eigenvalues	Eigenvectors	Remark
0	m zero eigenvalues	Of the form $[\mathbf{0}; \mathbf{b}]$ where \mathbf{b} is in \mathcal{N} and is given by $\begin{bmatrix} \boldsymbol{\varphi}_1 \\ \vdots \\ \boldsymbol{\varphi}_m \end{bmatrix}, \begin{bmatrix} \boldsymbol{\varphi}_2 \\ \vdots \\ \boldsymbol{\varphi}_m \end{bmatrix}, \dots, \begin{bmatrix} \boldsymbol{\varphi}_m \end{bmatrix}$	- arise from norm constraints on mode shapes; - carry no ID uncertainty
1	$m(n-m)$ eigenvalues, equal to λ_i (multiplicity $n-m$), $i=1, \dots, m$	Of the form $[\mathbf{0}; \mathbf{b}]$ where \mathbf{b} is in \mathcal{M}_\perp and is given by $\mathbf{a}_i \otimes \mathbf{b}_j$, $i=1, \dots, m$; $j=1, \dots, n-m$; $\{\mathbf{a}_i\}_{i=1}^m$ are eigenvectors of $2S_e^{-1} \text{Re} \Sigma \mathbf{H}_k$ with eigenvalues $\{\lambda_i\}_{i=1}^m$; $\{\mathbf{b}_j\}_{j=1}^{n-m}$ are the $(n-m)$ eigenvectors of \mathbf{Q} with eigenvalue 1	- induce ID uncertainty of mode shape perpendicular to MSS - induce no ID uncertainty in other parameters - found previously in single mode - induced uncertainty vanishes for noiseless data, negligible for high s/n ratio
2	$(m+1)^2 + m(m-1)$ eigenvalues, equal to those of the eigenvalue problem $\mathbf{J}_c \mathbf{x} = \lambda \mathbf{B} \mathbf{x}$ in (25)	Of the form $\boldsymbol{\theta} = [\mathbf{a}; \mathbf{b}]$, where $\mathbf{b} = \mathbf{U} \boldsymbol{\alpha}$ is in \mathcal{M} ; \mathbf{U} contains a basis for \mathcal{M} ; $\mathbf{x} = [\mathbf{a}; \boldsymbol{\alpha}]$ is eigenvector of the eigenvalue problem $\mathbf{J}_c \mathbf{x} = \lambda \mathbf{B} \mathbf{x}$ in (25)	- induce ID uncertainty of mode shape within MSS; - correlated with ID uncertainty of other parameters; - not found in single mode, new discovery unique to close modes; - induced uncertainty does not vanish for noiseless data, can be significant regardless of s/n ratio

280 6 Outline of derivations

281 The FIM in (3) is a generic expression that does not tell how it depends on modal properties, which
 282 can be very complicated in general situations. In this section we outline the derivation of the explicit
 283 expressions for the FIM in Table 2, which are asymptotically correct for high s/n ratio, i.e., as the
 284 noise PSD $S_e \rightarrow 0$. The first step is to approximate the inverse of $\mathbf{E}_k = \overline{\Phi} \mathbf{H}_k \overline{\Phi}^T + S_e \mathbf{I}_n$ in (1) by
 285 a Taylor expansion for small S_e . For this purpose, one should not take $\mathbf{E}_k \sim \overline{\Phi} \mathbf{H}_k \overline{\Phi}^T$ because
 286 $\overline{\Phi} \mathbf{H}_k \overline{\Phi}^T$ is rank deficient. One proper way is to use the matrix inverse lemma [30][31] to obtain

$$287 \mathbf{E}_k^{-1} = S_e^{-1} (\mathbf{I}_n - \overline{\Phi} \mathbf{P}_k^{-1} \overline{\Phi}^T) \quad (6)$$

288 where

$$289 \mathbf{P}_k = \overline{\Phi}^T \overline{\Phi} + S_e \mathbf{H}_k^{-1} \quad (7)$$

290 Assuming $n \geq m$ and the columns of $\overline{\Phi}$ are linearly independent, $\overline{\Phi}^T \overline{\Phi}$ ($m \times m$) has full rank and
 291 so $\mathbf{P}_k \sim \overline{\Phi}^T \overline{\Phi}$ is a legitimate 0th order approximation. However, it turns out that this does not give
 292 the correct approximation for \mathbf{E}_k^{-1} w.r.t. parameters affecting \mathbf{H}_k . Up to second order,

$$293 \mathbf{P}_k^{-1} \sim (\overline{\Phi}^T \overline{\Phi})^{-1} [\overline{\Phi}^T \overline{\Phi} - \boldsymbol{\varepsilon}_k + \boldsymbol{\varepsilon}_k (\overline{\Phi}^T \overline{\Phi})^{-1} \boldsymbol{\varepsilon}_k] (\overline{\Phi}^T \overline{\Phi})^{-1} \quad \boldsymbol{\varepsilon}_k = S_e \mathbf{H}_k^{-1} \quad (8)$$

294 Substituting into (6) gives

$$295 \mathbf{E}_k^{-1} \sim \underbrace{S_e^{-1} \mathbf{Q}}_{0\text{th order}} + \underbrace{S_e^{-1} \mathbf{R}^T \boldsymbol{\varepsilon}_k \mathbf{R}}_{1\text{st order}} - \underbrace{S_e^{-1} \mathbf{R}^T \boldsymbol{\varepsilon}_k (\overline{\Phi}^T \overline{\Phi})^{-1} \boldsymbol{\varepsilon}_k \mathbf{R}}_{2\text{nd order}} \quad (9)$$

296 where $\mathbf{Q} = \mathbf{I}_n - \overline{\Phi} (\overline{\Phi}^T \overline{\Phi})^{-1} \overline{\Phi}^T$ was defined in (4); and

$$297 \mathbf{R} = (\overline{\Phi}^T \overline{\Phi})^{-1} \overline{\Phi}^T \quad (10)$$

298 The matrices \mathbf{Q} and \mathbf{R} appear frequently in the derivation and their properties are worth-noting.
 299 First, $\mathbf{R} \overline{\Phi} = \mathbf{I}_m$ and $\mathbf{R} \mathbf{u} = \mathbf{0}$ for any \mathbf{u} orthogonal to the ‘mode shape subspace’ (MSS), i.e., space
 300 spanned by mode shapes $\{\overline{\boldsymbol{\varphi}}_i\}_{i=1}^m$. The matrix \mathbf{Q} is a zero mapping in the MSS and an identity
 301 mapping in the orthogonal complement of MSS. The zero mapping can be seen from $\mathbf{Q} \overline{\Phi} = \mathbf{0}$. The
 302 identity mapping can be seen from $\overline{\Phi}^T \mathbf{u} = \mathbf{0}$ for any \mathbf{u} orthogonal to MSS. These properties imply
 303 that \mathbf{Q} has m zero eigenvalues with an orthogonal basis of eigenvectors in the MSS. The remaining
 304 $n - m$ eigenvalues are all equal to 1 with an orthogonal basis of eigenvectors in the orthogonal
 305 complement of the MSS.

306 The derivatives in (3) w.r.t. different groups of parameters are given by

$$307 \quad \mathbf{E}_k^{(x)} = \overline{\Phi} \mathbf{H}_k^{(x)} \overline{\Phi}^T \quad (x = f, \zeta, \mathbf{S}) \quad \mathbf{E}_k^{(S_e)} = \mathbf{I}_n \quad (11)$$

$$308 \quad \mathbf{E}_k^{(\Phi_{ri})} = \overline{\Phi}^{(\Phi_{ri})} \mathbf{H}_k \overline{\Phi}^T + \overline{\Phi} \mathbf{H}_k \overline{\Phi}^{(\Phi_{ri})} \quad (12)$$

309 where Φ_{ri} denotes the (r, i) -entry of Φ . Using (9) and (11), considering the leading order terms
 310 and simplifying gives J_{xy} , J_{xS_e} and $J_{S_e S_e}$ in Table 2 ($x, y = \{f, \zeta, \mathbf{S}\}$). Details can be found in
 311 Section 13. For the entries in FIM related to mode shapes, using (12), considering the leading order
 312 terms and simplifying gives (see Section 14 for details):

$$313 \quad J_{x\Phi_{ri}} \sim 2 \text{Re} \text{tr} \Sigma [\mathbf{H}_k^{(x)} \mathbf{H}_k^{-1} \mathbf{R} \overline{\Phi}^{(\Phi_{ri})}] \quad x = f, \zeta, \mathbf{S} \quad (13)$$

$$314 \quad J_{S_e \Phi_{ri}} \sim 2 \text{Re} \text{tr} \Sigma [(\overline{\Phi}^T \overline{\Phi})^{-1} \mathbf{H}_k^{-1} \mathbf{R} \overline{\Phi}^{(\Phi_{ri})}] \quad (14)$$

$$315 \quad J_{xy} \sim J_{xy}^{(1)} + J_{xy}^{(2)} \quad x, y = \Phi \quad (15)$$

316 where ' $x, y = \Phi$ ' denotes that x and y are entries in Φ ; and

$$317 \quad J_{xy}^{(1)} = 2S_e^{-1} \text{tr} [\mathbf{Q} \overline{\Phi}^{(x)} (\text{Re} \Sigma \mathbf{H}_k) \overline{\Phi}^{(y)T}] \quad x, y = \Phi \quad (16)$$

$$318 \quad J_{xy}^{(2)} = 2N_f \text{tr} [\mathbf{R} \overline{\Phi}^{(x)} \mathbf{R} \overline{\Phi}^{(y)}] + 2 \text{Re} \text{tr} \Sigma [\mathbf{R}^T \mathbf{H}_k^{-1} \mathbf{R} \overline{\Phi}^{(x)} \mathbf{H}_k \overline{\Phi}^{(y)T}] \quad x, y = \Phi \quad (17)$$

319 To express in more explicit form, the derivative $\overline{\Phi}^{(\Phi_{ri})}$ from (61) in Appendix I of [22] is used:

$$320 \quad \overline{\Phi}^{(\Phi_{ri})} = [\overline{\Phi}_1^{(\Phi_{ri})} \quad \dots \quad \overline{\Phi}_m^{(\Phi_{ri})}] = \|\boldsymbol{\varphi}_i\|^{-1} (\mathbf{I}_n - \overline{\boldsymbol{\varphi}}_i \overline{\boldsymbol{\varphi}}_i^T) \mathbf{e}_r \mathbf{e}_i^T \quad (18)$$

321 Substituting (18) into (13) to (17), considering the leading order term, simplifying and assembling in
 322 matrix form gives the final expressions of $J_{x\boldsymbol{\varphi}_i}$, $J_{S_e \boldsymbol{\varphi}_i}$ and $J_{\Phi:\Phi}$ in Table 2. See Section 15 for
 323 details.

324 **7 Principal subspaces of mode shape uncertainty**

325 The eigenvalue properties of the high s/n asymptotic FIM in Table 2 will be investigated analytically
 326 in Section 8. For this purpose, some important concepts are reviewed/introduced in this section. The
 327 mode shape $\boldsymbol{\varphi}_i$ of a particular mode i is an $n \times 1$ vector in the n -dimensional Euclidean space,
 328 denoted by R^n . The mode shape subspace (MSS), denoted by \mathcal{M} , is the subspace in R^n spanned
 329 by $\{\boldsymbol{\varphi}_1, \dots, \boldsymbol{\varphi}_m\}$, i.e., the collection of all vectors of the form $\mathbf{x} = \sum_{i=1}^m a_i \boldsymbol{\varphi}_i$ where $\{a_i\}_{i=1}^m$ are real

330 numbers. The orthogonal complement of \mathcal{M} , denoted by \mathcal{M}_\perp , is the subspace in R^n comprising all
331 vectors orthogonal to those in \mathcal{M} , i.e., the collection of all vectors \mathbf{y} such that $\mathbf{y}^T \mathbf{x} = 0$ for any \mathbf{x}
332 in \mathcal{M} . Assuming $\{\boldsymbol{\varphi}_1, \dots, \boldsymbol{\varphi}_m\}$ are linearly independent, \mathcal{M} has dimension m and \mathcal{M}_\perp has
333 dimension $n - m$. Symbolically this can be written as $R^n = \mathcal{M} + \mathcal{M}_\perp$. The same is also true for their
334 dimensions, i.e., $n = m + (n - m)$. For a given i , let $\{\mathbf{u}_{ij}\}_{j=1}^{m-1}$ be a basis in the orthogonal
335 complement of $\boldsymbol{\varphi}_i$ in \mathcal{M} . That is, $\boldsymbol{\varphi}_i$ and $\{\mathbf{u}_{ij}\}_{j=1}^{m-1}$ form a basis in \mathcal{M} but $\boldsymbol{\varphi}_i$ is orthogonal to \mathbf{u}_{ij} .
336 Let also $\{\mathbf{v}_{ij}\}_{j=1}^{n-m}$ be a basis in \mathcal{M}_\perp . Then $\boldsymbol{\varphi}_i$, $\{\mathbf{u}_{ij}\}_{j=1}^{m-1}$ and $\{\mathbf{v}_{ij}\}_{j=1}^{n-m}$ together form a basis in R^n .

337 As a note, $\{\mathbf{u}_{ij}\}_{j=1}^{m-1}$ are linearly independent but need not be orthogonal. One geometrically
338 intuitive possibility is for \mathbf{u}_{ij} to be a vector along the tangential direction from $\boldsymbol{\varphi}_i$ that rotates from
339 $\boldsymbol{\varphi}_i$ towards $\boldsymbol{\varphi}_j$ in the hyperplane formed by them:

$$340 \quad \mathbf{u}_{ij} = \boldsymbol{\varphi}_j - \boldsymbol{\varphi}_i r_{ij} \quad r_{ij} = \frac{\boldsymbol{\varphi}_i^T \boldsymbol{\varphi}_j}{\boldsymbol{\varphi}_i^T \boldsymbol{\varphi}_i} \quad j \neq i \quad (19)$$

341 As a check, \mathbf{u}_{ij} lies in the plane formed by $\boldsymbol{\varphi}_i$ and $\boldsymbol{\varphi}_j$; and $\boldsymbol{\varphi}_i^T \mathbf{u}_{ij} = 0$. Another possibility is for
342 $\{\mathbf{u}_{ij}\}_{j=1}^{m-1}$ to be a set of orthogonal basis from the Gram-Schmidt procedure [30]. The choice of
343 $\{\mathbf{u}_{ij}\}_{j=1}^{m-1}$ is discussed here for concreteness only. It does not affect the theory developed.

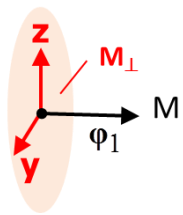
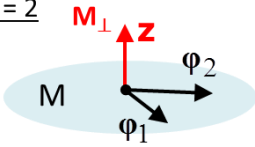
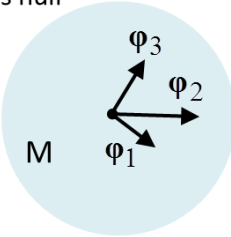
344 The $n \times n$ posterior covariance matrix of $\boldsymbol{\varphi}_i$ only informs the uncertainty of $\boldsymbol{\varphi}_i$ but not its
345 correlation with other mode shapes. A complete description of the uncertainty with m modes
346 requires one to study the $mn \times mn$ posterior covariance matrix of the $mn \times 1$ vector
347 $\boldsymbol{\Phi} := [\boldsymbol{\varphi}_1; \dots; \boldsymbol{\varphi}_m]$, (';' denotes stacking column-wise). Although it may appear artificial at this stage,
348 it is useful to introduce three orthogonally complementary spaces in R^{mn} , namely, \mathcal{N} , \mathcal{M} and
349 \mathcal{M}_\perp , which are induced by $\boldsymbol{\varphi}_i$, \mathbf{u}_{ij} and \mathbf{v}_{ij} , respectively. They are defined in the first three
350 columns of Table 4; the remaining columns will become apparent in Section 8. Symbolically,
351 $R^{mn} = \mathcal{N} + \mathcal{M} + \mathcal{M}_\perp$. In the basis vector for \mathcal{N} , the Kronecker product $\mathbf{e}_i \otimes \boldsymbol{\varphi}_i$ ($mn \times 1$) puts $\boldsymbol{\varphi}_i$
352 in the i th partition and the remaining $(m-1)$ partitions (each $n \times 1$) are all zero. Similarly, the basis
353 vectors $\mathbf{e}_i \otimes \mathbf{u}_{ij}$ (for \mathcal{M}) and $\mathbf{e}_i \otimes \mathbf{v}_{ij}$ (for \mathcal{M}_\perp) have their i th partition equal to \mathbf{u}_{ij} and \mathbf{v}_{ij} ,
354 respectively; and the remaining partitions are zero. Figure 3 illustrates the three subspaces. As we
355 will see in Section 8, \mathcal{N} is associated with mode shape norm constraint and carries no uncertainty;

356 \mathcal{M} is associated with mode shape uncertainty within the MSS; \mathcal{M}_\perp is associated with uncertainty
357 orthogonal to the MSS.

358 **Table 4 Principal subspaces of mode shape uncertainty in R^{mn} ; MSS = mode shape subspace**

Subspace	Dimension	Basis	$J_{\Phi:\Phi}^{(1)}$	$J_{\Phi:\Phi}^{(2)}$	$J_{\Phi:\Phi}$	Remark
\mathcal{N}	m	$\mathbf{e}_i \otimes \boldsymbol{\varphi}_i$ $i = 1, \dots, m$	Null space	Null space	Null space	Norm-constrained subspace
\mathcal{M}	$m(m-1)$	$\mathbf{e}_i \otimes \mathbf{u}_{ij}$ $i, j = 1, \dots, m$ $j \neq i$	Null space	Non-zero eigenvalues, non-trivial	Eigenvalues and eigenvectors equal to those of $J_{\Phi:\Phi}^{(2)}$ in this space	Subspace containing all possible mode shape deviations within MSS
\mathcal{M}_\perp	$m(n-m)$	$\mathbf{e}_i \otimes \mathbf{v}_{ij}$ $i = 1, \dots, m$ $j = 1, \dots, n-m$	Eigenvalues equal to those of $2S_e^{-1} \text{Re} \Sigma \mathbf{H}_k$, each with multiplicity $n-m$	Null space	Eigenvalues and eigenvectors equal to those of $J_{\Phi:\Phi}^{(1)}$ in this space	Subspace containing all possible mode shape deviations orthogonal to MSS

359 **Figure 3 Example of basis for \mathcal{N} , \mathcal{M} and \mathcal{M}_\perp for $n=3$ measured DOFs and different number of**
 360 **modes m . When $m=1$, \mathcal{M} (mode shape subspace) is the line along φ_1 ; when $m=2$, \mathcal{M} is the**
 361 **2-D plane spanned by φ_1 and φ_2 ; when $m=3$, \mathcal{M} is the whole 3-D space; $r_{ij} = (\varphi_i^T \varphi_j) / (\varphi_i^T \varphi_i)$**

	\mathcal{N} Dim. m	\mathcal{M} Dim. $m(m-1)$	\mathcal{M}_\perp Dim. $m(n-m)$
$m=1$ 	Dim. = 1 φ_1	Dim. = 0 Null	Dim. = 2 z, y
$m=2$ 	Dim. = 2 $\begin{bmatrix} \varphi_1 \\ 0 \end{bmatrix}, \begin{bmatrix} 0 \\ \varphi_2 \end{bmatrix}$	Dim. = 2 $\begin{bmatrix} \varphi_2 - \varphi_1^T \varphi_2 \\ 0 \end{bmatrix}, \begin{bmatrix} 0 \\ \varphi_1 - \varphi_2^T \varphi_1 \end{bmatrix}$	Dim. = 2 $\begin{bmatrix} z \\ 0 \end{bmatrix}, \begin{bmatrix} 0 \\ z \end{bmatrix}$
$m=3$ \mathcal{M}_\perp is null 	Dim. = 3 $\begin{bmatrix} \varphi_1 \\ 0 \\ 0 \end{bmatrix}, \begin{bmatrix} 0 \\ \varphi_2 \\ 0 \end{bmatrix}, \begin{bmatrix} 0 \\ 0 \\ \varphi_3 \end{bmatrix}$	Dim. = 6 $\begin{bmatrix} \varphi_2 - \varphi_1^T \varphi_2 \\ 0 \\ 0 \end{bmatrix}, \begin{bmatrix} \varphi_3 - \varphi_1^T \varphi_3 \\ 0 \\ 0 \end{bmatrix}$ $\begin{bmatrix} 0 \\ \varphi_1 - \varphi_2^T \varphi_1 \\ 0 \end{bmatrix}, \begin{bmatrix} 0 \\ \varphi_3 - \varphi_2^T \varphi_3 \\ 0 \end{bmatrix}$ $\begin{bmatrix} 0 \\ 0 \\ \varphi_1 - \varphi_3^T \varphi_1 \end{bmatrix}, \begin{bmatrix} 0 \\ 0 \\ \varphi_2 - \varphi_3^T \varphi_2 \end{bmatrix}$	Dim. = 0 Null

362

363 8 Eigenvalue properties

364 In the derivation of uncertainty laws the mode shapes always present the major hurdle because of
 365 their dimension growing with the number of DOFs. For well-separated modes this has been resolved
 366 by discovering that the mode shape is asymptotically uncorrelated from the remaining parameters.
 367 Numerical experiments reveal that this is not the case for close modes and the correlation structure
 368 is non-trivial. In this section we analyse analytically, in turn, the eigenvalue properties of $\mathbf{J}_{\Phi:\Phi}^{(1)}$,
 369 $\mathbf{J}_{\Phi:\Phi}^{(2)}$, $\mathbf{J}_{\Phi:\Phi}$ and the full FIM \mathbf{J} in Table 2; and finally the high s/n asymptotic posterior covariance
 370 matrix $\mathbf{C} = \mathbf{J}^{-1}$. This allows us to understand the principal directions in which the ID uncertainty of
 371 modal parameters, especially the mode shapes, takes place. As we will see, the results are
 372 remarkably definitive and characteristic, despite complexity of the close modes problem and the
 373 mathematics involved.

374 8.1 $\mathbf{J}_{\Phi:\Phi}^{(1)}$ (Type 1)

375 The eigenvalue properties of $\mathbf{J}_{\Phi:\Phi}^{(1)}$ follow directly from the standard result in linear algebra that if
376 A ($m \times m$) has eigenvalue a_i with eigenvector u_i ($i = 1, \dots, m$) and B ($n \times n$) has eigenvalue b_j
377 with eigenvector v_j ($j = 1, \dots, n$) then the Kronecker product $A \otimes B$ has eigenvalue $a_i b_j$ with
378 eigenvector $u_i \otimes v_j$ ($i = 1, \dots, m; j = 1, \dots, n$). Applying this result, the eigenvalues of $\mathbf{J}_{\Phi:\Phi}^{(1)}$ are the
379 product of those of $2S_e^{-1} \text{Re}\Sigma\mathbf{H}_k$ and \mathbf{Q} . The eigenvectors are the Kronecker product of the
380 eigenvectors of $2S_e^{-1} \text{Re}\Sigma\mathbf{H}_k$ and \mathbf{Q} . Since \mathbf{Q} has m zero eigenvalues with eigenvectors
381 $\{\boldsymbol{\varphi}_1, \dots, \boldsymbol{\varphi}_m\}$, $\mathbf{J}_{\Phi:\Phi}^{(1)}$ has m^2 zero eigenvalues. The basis vectors $\{\mathbf{e}_i \otimes \boldsymbol{\varphi}_i\}_{i=1}^m$ of \mathcal{N} are among the
382 eigenvectors with zero eigenvalue, which can be verified by direct substitution and noting that
383 $\mathbf{Q}_i \boldsymbol{\varphi}_i = \mathbf{0}$. In general, for the zero eigenvalues, resulting from Kronecker product the i th partition
384 of the eigenvector is a multiple of $\boldsymbol{\varphi}_i$ and hence lies in the MSS. Since a linear combination of
385 eigenvectors of the same eigenvalue is also an eigenvector, in the context of Table 4 the zero
386 eigenvalue can be considered to have m eigenvectors in \mathcal{N} and $m(m-1)$ eigenvectors in \mathcal{M} .

387 Other than the zero eigenvalue, the remaining $(n-m)$ eigenvalues of \mathbf{Q} are all equal to 1 with
388 eigenvectors in M_{\perp} . The remaining $m(n-m)$ eigenvalues of $\mathbf{J}_{\Phi:\Phi}^{(1)}$ are then equal to the m
389 eigenvalues of $2S_e^{-1} \text{Re}\Sigma\mathbf{H}_k$, each with multiplicity (i.e., repeating) $n-m$. The eigenvectors of this
390 type lie in the orthogonal complement of \mathcal{N} and \mathcal{M} , i.e., \mathcal{M}_{\perp} . These results are summarised in the
391 fourth column of Table 4.

392 8.2 $\mathbf{J}_{\Phi:\Phi}^{(2)}$ (Type 2)

393 The eigenvalue properties of $\mathbf{J}_{\Phi:\Phi}^{(2)}$ are complementary to $\mathbf{J}_{\Phi:\Phi}^{(1)}$. The $m(n-m)$ eigenvectors of
394 $\mathbf{J}_{\Phi:\Phi}^{(1)}$ with non-zero eigenvalue (hence in \mathcal{M}_{\perp}) are eigenvectors of $\mathbf{J}_{\Phi:\Phi}^{(2)}$ with zero eigenvalue. To
395 see this, such an eigenvector is of the form $\mathbf{v} = [a_1 \mathbf{u}; \dots; a_m \mathbf{u}]$ (';' denotes stacking column-wise),
396 where $[a_1, \dots, a_m]^T$ is an eigenvector of $2S_e^{-1} \text{Re}\Sigma\mathbf{H}_k$ and \mathbf{u} is an eigenvector of \mathbf{Q} with
397 eigenvalue 1, i.e., in M_{\perp} . Then $\overline{\boldsymbol{\Phi}}^T \mathbf{u} = \mathbf{0}$ and $\overline{\boldsymbol{\varphi}}_i^T \mathbf{u} = 0$, and from (5) we can deduce $\mathbf{Q}_i \mathbf{u} = \mathbf{0}$. This
398 implies that

$$399 \begin{bmatrix} \mathbf{Q}_1 & & \\ & \ddots & \\ & & \mathbf{Q}_m \end{bmatrix} \begin{bmatrix} a_1 \mathbf{u} \\ \vdots \\ a_m \mathbf{u} \end{bmatrix} = \begin{bmatrix} a_1 \mathbf{Q}_1 \mathbf{u} & & \\ & \ddots & \\ & & a_m \mathbf{Q}_m \mathbf{u} \end{bmatrix} = \mathbf{0} \quad (20)$$

400 and so from the expression of $J_{\Phi:\Phi}^{(2)}$ in Table 2 we can deduce $J_{\Phi:\Phi}^{(2)}\mathbf{u} = \mathbf{0}$. By a similar argument,
 401 the vectors in \mathcal{N} are also null vectors of $J_{\Phi:\Phi}^{(2)}$. Consequently, $J_{\Phi:\Phi}^{(2)}$ only has
 402 $mn - m(n - m) - m = m(m - 1)$ possibly non-zero eigenvalues whose eigenvectors lie in the
 403 orthogonal complement of both \mathcal{N} and \mathcal{M}_\perp , i.e., \mathcal{M} . These results are summarised in the fifth
 404 column of Table 4.

405 **8.3 Mode shape FIM $J_{\Phi:\Phi}$:**

406 The eigenvalue properties of $J_{\Phi:\Phi}$ inherit directly from those of $J_{\Phi:\Phi}^{(1)}$ and $J_{\Phi:\Phi}^{(2)}$. The null space
 407 \mathcal{N} is common to $J_{\Phi:\Phi}^{(1)}$ and $J_{\Phi:\Phi}^{(2)}$ and is therefore also a null space for $J_{\Phi:\Phi}$. In \mathcal{M} where
 408 $J_{\Phi:\Phi}^{(1)}$ is a zero mapping, the eigenvalues and eigenvectors of $J_{\Phi:\Phi}$ directly inherit from those of
 409 $J_{\Phi:\Phi}^{(2)}$. To see this, if \mathbf{u} in \mathcal{M} is an eigenvector of $J_{\Phi:\Phi}^{(2)}$ with eigenvalue λ , then $J_{\Phi:\Phi}^{(1)}\mathbf{u} = \mathbf{0}$ and
 410 $J_{\Phi:\Phi}^{(2)}\mathbf{u} = \lambda\mathbf{u}$, and so $J_{\Phi:\Phi}\mathbf{u} = J_{\Phi:\Phi}^{(1)}\mathbf{u} + J_{\Phi:\Phi}^{(2)}\mathbf{u} = \lambda\mathbf{u}$, i.e., \mathbf{u} is also an eigenvector of $J_{\Phi:\Phi}$
 411 with the same eigenvalue λ . By the same argument, in \mathcal{M}_\perp where $J_{\Phi:\Phi}^{(2)}$ is a zero mapping, the
 412 eigenvalues and eigenvectors of $J_{\Phi:\Phi}$ inherit directly from those of $J_{\Phi:\Phi}^{(1)}$. These are summarised
 413 in the sixth column of Table 4.

414 **8.4 Full FIM \mathbf{J}**

415 The eigenvalue properties of the full FIM \mathbf{J} can be reasoned from those of $J_{\Phi:\Phi}$. Let ϖ be a
 416 vector containing all parameters other than mode shapes so that $\boldsymbol{\theta} = [\varpi; \Phi;]$ contains all modal
 417 parameters and \mathbf{J} is the full FIM w.r.t. $\boldsymbol{\theta}$. Let $\mathbf{v} = [\mathbf{v}_1; \dots; \mathbf{v}_m]$ be an eigenvector of $J_{\Phi:\Phi}$ with
 418 eigenvalue λ and it lies either in \mathcal{N} (dim. m , Type 0) or \mathcal{M}_\perp (dim. $m(n - m)$, Type 1). When \mathbf{v} is
 419 in \mathcal{N} , $\mathbf{v}_i \propto \boldsymbol{\phi}_i$; when \mathbf{v} is in \mathcal{M}_\perp , \mathbf{v}_i is in M_\perp . In either case $\mathbf{Q}_i\mathbf{v}_i = \mathbf{0}$. For all remaining
 420 parameters x from ϖ , $J_{x\varphi_i}$ has \mathbf{Q}_i on its right end (see Table 2) and so

421 $J_{x\Phi}\mathbf{v} = [J_{x\varphi_1}\mathbf{v}_1, \dots, J_{x\varphi_m}\mathbf{v}_m] = \mathbf{0}$. Then

$$422 \quad \mathbf{J} \begin{bmatrix} \mathbf{0} \\ \mathbf{v} \end{bmatrix} = \begin{bmatrix} J_{\varpi\varpi} & J_{\varpi\Phi} \\ J_{\varpi\Phi}^T & J_{\Phi:\Phi} \end{bmatrix} \begin{bmatrix} \mathbf{0} \\ \mathbf{v} \end{bmatrix} = \begin{bmatrix} J_{\varpi\Phi}\mathbf{v} \\ J_{\Phi:\Phi}\mathbf{v} \end{bmatrix} = \lambda \begin{bmatrix} \mathbf{0} \\ \mathbf{v} \end{bmatrix} \quad (\mathbf{v} \text{ in } \mathcal{N} \text{ or } \mathcal{M}_\perp) \quad (21)$$

423 This implies that \mathbf{J} has $m + m(n - m)$ eigenvectors of the form $[\mathbf{0}; \mathbf{v}]$, i.e., where mode shape
 424 uncertainty is uncoupled from all other parameters.

425 There remains $(m + 1)^2 + m(m - 1)$ eigenvalues. They all contribute to mode shape uncertainties in
 426 \mathcal{M} , i.e., Type 2. To see this, let the eigenvector be partitioned as $\boldsymbol{\theta} = [\mathbf{a}; \mathbf{b}]$ where \mathbf{a} is $(m + 1)^2$

427 dimensional for ϖ and \mathbf{b} is mn dimensional for Φ :. Since all eigenvectors of (real-symmetric) \mathbf{J}
 428 are orthogonal, $\boldsymbol{\theta} = [\mathbf{a}; \mathbf{b}]$ must be orthogonal to $[\mathbf{0}; \mathbf{v}]$ where \mathbf{v} is in \mathcal{N} or \mathcal{M}_\perp . This implies
 429 $\mathbf{v}^T \mathbf{b} = 0$. As \mathbf{v} lies in the subspace formed by \mathcal{N}_1 and \mathcal{M}_\perp , \mathbf{b} must lie in the orthogonal
 430 complement of this subspace, i.e., \mathcal{M} .

431 8.5 Condensed eigenvalue problem for Type 2

432 The eigenvalue properties of Type 2 can be found from an eigenvalue problem of reduced dimension.
 433 Essentially, one can represent \mathbf{b} in $\boldsymbol{\theta} = [\mathbf{a}; \mathbf{b}]$ as a linear combination of basis vectors in \mathcal{M} , i.e.,

$$434 \quad \mathbf{b} = \begin{bmatrix} \mathbf{U}_1 \mathbf{a}_1 \\ \vdots \\ \mathbf{U}_m \mathbf{a}_m \end{bmatrix} = \underbrace{\begin{bmatrix} \mathbf{U}_1 & & \\ & \ddots & \\ & & \mathbf{U}_m \end{bmatrix}}_{\mathbf{U}} \underbrace{\begin{bmatrix} \mathbf{a}_1 \\ \vdots \\ \mathbf{a}_m \end{bmatrix}}_{\boldsymbol{\alpha}} \quad (22)$$

435 where \mathbf{U}_i is a $n \times (m-1)$ matrix containing in its columns the basis $\{\mathbf{u}_{ij}\}_{j=1}^{m-1}$ in \mathcal{M} but orthogonal
 436 to $\boldsymbol{\phi}_i$ (see Section 7) and \mathbf{a}_i is a $(m-1) \times 1$ vector containing the coordinates w.r.t. the basis.
 437 Determining \mathbf{b} (dim. mn) reduces to determining $\boldsymbol{\alpha}$. An eigenvector of Type 2 can then be
 438 represented as

$$439 \quad \mathbf{v} = \begin{bmatrix} \mathbf{a} \\ \mathbf{U} \boldsymbol{\alpha} \end{bmatrix} = \begin{bmatrix} \mathbf{I} \\ \mathbf{U} \end{bmatrix} \begin{bmatrix} \mathbf{a} \\ \boldsymbol{\alpha} \end{bmatrix} \quad (23)$$

440 For $\boldsymbol{\theta} = [\varpi; \Phi:]$, the eigenvalue problem for \mathbf{J} involving eigenvectors of Type 2 reads

$$441 \quad \begin{bmatrix} J_{\varpi\varpi} & J_{\varpi\Phi} \\ J_{\Phi:\varpi} & J_{\Phi:\Phi} \end{bmatrix} \begin{bmatrix} \mathbf{I} \\ \mathbf{U} \end{bmatrix} \begin{bmatrix} \mathbf{a} \\ \boldsymbol{\alpha} \end{bmatrix} = \lambda \begin{bmatrix} \mathbf{I} \\ \mathbf{U} \end{bmatrix} \begin{bmatrix} \mathbf{a} \\ \boldsymbol{\alpha} \end{bmatrix} \quad (24)$$

442 Left-multiplying by the transpose of the first matrix on the right hand side gives the generalised
 443 eigenvalue problem

$$444 \quad \mathbf{J}_c \mathbf{x} = \lambda \mathbf{B} \mathbf{x} \quad (25)$$

$$445 \quad \mathbf{J}_c = \begin{bmatrix} J_{\varpi\varpi} & J_{\varpi\Phi} \mathbf{U} \\ \mathbf{U}^T J_{\Phi:\varpi} & \mathbf{U}^T J_{\Phi:\Phi} \mathbf{U} \end{bmatrix} \quad \mathbf{B} = \begin{bmatrix} \mathbf{I} \\ \mathbf{U}^T \mathbf{U} \end{bmatrix} \quad \mathbf{x} = \begin{bmatrix} \mathbf{a} \\ \boldsymbol{\alpha} \end{bmatrix} \quad (26)$$

446 Note that \mathbf{J}_c has full rank. The original eigenvalue problem with \mathbf{J} of dimension $(m+1)^2 + mn$ is
 447 now reduced to one with \mathbf{J}_c of dimension $(m+1)^2 + m(m-1)$, which does not depend on the
 448 number of measured DOFs n . The complexity w.r.t. n is resolved and consolidated into the
 449 associated coordinates in $\boldsymbol{\alpha}$. The eigenvalue properties of \mathbf{J} are summarised in Table 3.

450 **8.6 High s/n asymptotic posterior covariance matrix**

451 The asymptotic posterior covariance matrix \mathbf{C} is equal to the inverse of the full FIM \mathbf{J} ignoring the
452 m zero eigenvalues associated with norm constraints, i.e., evaluated as a pseudo-inverse via
453 eigenvector representation ignoring the zero eigenvalues. It inherits the eigenvectors of \mathbf{J} and its
454 eigenvalues are equal to the reciprocal of those of \mathbf{J} , except for the m zero eigenvalues. It has m
455 zero eigenvalues (Type 0) associated with norm constraints. Another $m(n - m)$ eigenvalues are
456 associated with mode shape uncertainty orthogonal to the MSS (Type 1), equal to $\{\lambda_i^{-1}\}_{i=1}^m$ (each
457 repeating $(n - m)$ times), where $\{\lambda_i\}_{i=1}^m$ are the eigenvalues of $2S_e^{-1} \mathbf{Re} \Sigma \mathbf{H}_k$. The remaining
458 $(m + 1)^2 + m(m - 1)$ eigenvalues are reciprocals of those of the eigenvalue problem in (25). These
459 are non-trivial and are associated potentially with all parameters correlated, i.e., no zeros in the
460 eigenvectors.

461 **9 Dominant mode shape uncertainty**

462 For well-separated modes it has been found in previous studies [23] that mode shape uncertainty is
463 inversely proportional to s/n ratio. Such uncertainty is perpendicular to the mode shape with a
464 variance proportional to the noise PSD. It is therefore typically small for data with good s/n ratio and
465 vanishes for noiseless data, despite the uncertainty in the excitation that remains. Intuitively, for
466 well-separated modes the mode shape values at different DOFs are directly related to their ratio of
467 data FFTs where the effect of the modal force is almost cancelled out when s/n ratio is high. For
468 noiseless data the ratio of data FFTs depends solely on the ratio of mode shape values and hence the
469 latter can be precisely determined (together with a scaling constraint). Except for the zero
470 eigenvalue associated with norm constraint, all other eigenvalues of the mode shape covariance
471 matrix are theoretically the same and hence there is no dominant direction of uncertainty. The
472 foregoing findings in this work reveal that this is not the case for close modes because the $m(m - 1)$
473 eigenvalues associated with uncertainty within MSS (Type 2) are significantly larger than the
474 $m(n - m)$ eigenvalues associated with uncertainty orthogonal to MSS (Type 1). The implication is
475 that for close modes the mode shape uncertainty does not vanish for noiseless data, which is a
476 consequence of the fact that the excitation is not known but modelled in a stochastic manner.

477 Let $\{\delta_i\}_{i=1}^{mm}$ and $\{\mathbf{u}_i\}_{i=1}^{mm}$ be respectively the eigenvalues and eigenvectors of the covariance matrix
478 of Φ . Given data, Φ is a Gaussian vector with mean equal to its MPV and uncertain deviation
479 $\Delta\Phi$: given by

$$480 \quad \Delta\Phi := \begin{bmatrix} \Delta\phi_1 \\ \vdots \\ \Delta\phi_m \end{bmatrix} = \sum_{i=1}^{mn} Z_i \sqrt{\delta_i} \mathbf{u}_i \quad (27)$$

481 where $\{Z_i\}_{i=1}^{mn}$ are i.i.d. standard Gaussian random variables. It can be easily verified that the
 482 covariance matrix of $\Delta\Phi$: is equal to the mode shape covariance matrix.

483 The foregoing findings imply that Φ : has $m(m-1)$ dominant uncertain directions within the MSS.
 484 The remaining directions are either asymptotically small (orthogonal to MSS, Type 1) for high s/n
 485 ratios or norm-constrained (m directions along MPV, Type 0). Analogous results apply to the mode
 486 shape ϕ_i ($n \times 1$) of a particular mode. It has $(m-1)$ dominant uncertain directions within the MSS
 487 (Type 2), $(n-m)$ directions orthogonal to the MSS (Type 1) and 1 direction along the MPV that is
 488 norm-constrained.

489 10 Illustrative examples

490 10.1 Verification

491 Here we verify numerically the eigenvalue properties of the mode shape FIM predicted in Section 8.

492 Consider two close modes with natural frequencies $f_1 = 1$ Hz and $f_2 = 1.05$ Hz, damping ratios

493 $\zeta_1 = 1\%$ and $\zeta_2 = 1.5\%$, modal force PSDs $S_{11} = S_{22} = 1(\mu\text{g})^2 / \text{Hz}$, modal force coherence

494 $\chi = S_{21} / \sqrt{S_{11}S_{22}} = 0.5e^{i\pi/4}$ and mode shapes (confined to measured DOFs) $\phi_1 = \mathbf{u}_1$ and

495 $\phi_2 = \rho\mathbf{u}_1 + \sqrt{1-\rho^2}\mathbf{u}_2$ where

$$496 \quad \mathbf{u}_1 = [1 \quad 2 \quad 3 \quad 4 \quad 5]^T / \sqrt{55} \quad \mathbf{u}_2 = [1 \quad 2 \quad 3 \quad 0 \quad -14/5]^T / \sqrt{21.48} \quad (28)$$

497 Check that \mathbf{u}_1 and \mathbf{u}_2 are orthogonal unit vectors and the MAC (modal assurance criterion)

498 between ϕ_1 and ϕ_2 is ρ , which is set to be 0.5. Data is acceleration of 1000 sec duration and

499 sampled at 10 Hz. It is contaminated with white noise of PSD S_e . The latter is set to be

500 $S_e = S_{11} / 4\zeta_1^2\gamma$ so that the s/n ratio in terms of PSD at the natural frequency of Mode 1 is γ ,

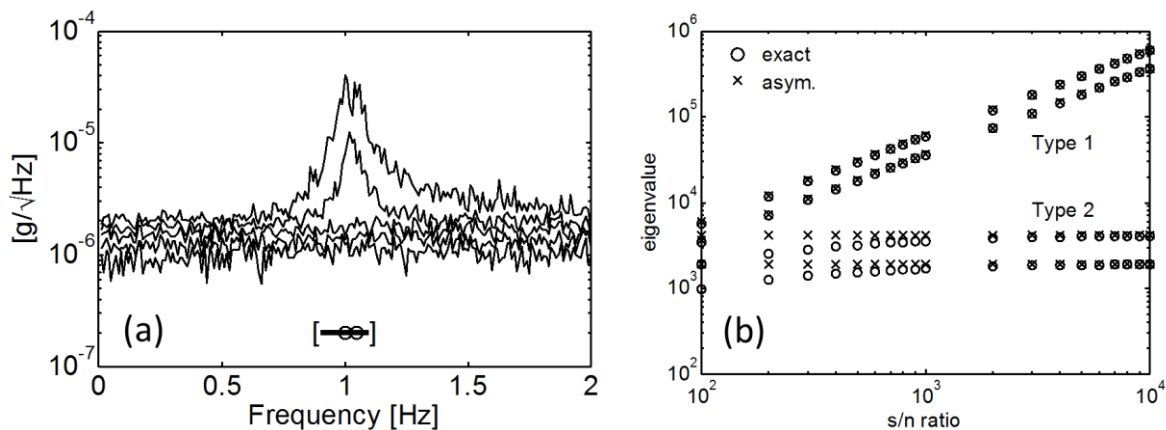
501 which will be varied in the study. The band from 0.9Hz to 1.1Hz is used for Bayesian modal ID. This

502 example focuses on verifying the mathematical correctness of the asymptotic FIM in Section 8. The

503 FIMs (asymptotic and exact) are evaluated directly at the actual values of modal properties. In

504 Section 10.2 with field data they will be evaluated at the MPV calculated for given data, which is the

505 best one can do when there is no ‘true’ parameter value. Nevertheless, to give an idea of how close
 506 the modes are in this example, Figure 4 shows the singular value (SV) spectrum of a typical set of
 507 synthetic data when the s/n ratio is 1000.



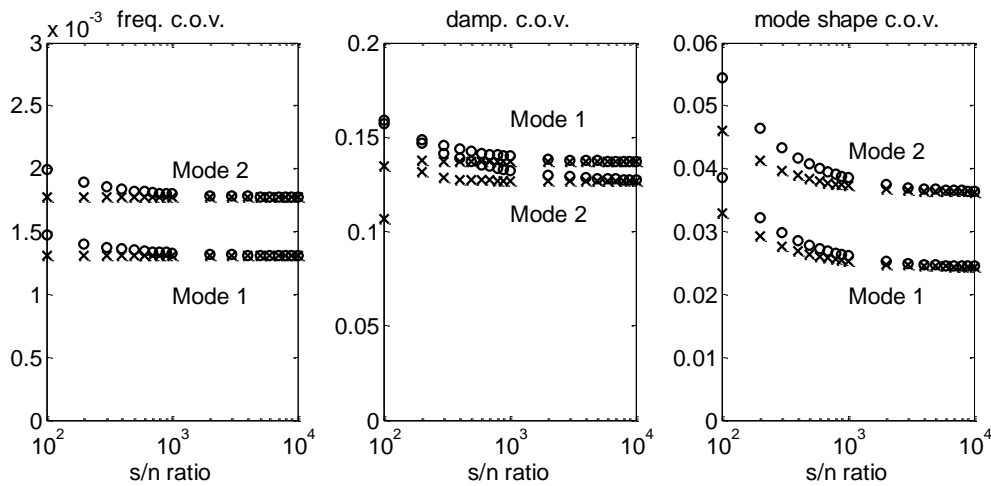
508
 509 **Figure 4 (a) Root SV spectrum of a typical set of synthetic data; (b) Eigenvalues of mode shape FIM**
 510 **$\mathbf{J}_{\Phi,\Phi}$.** Circle – exact based on (3); cross – high s/n asymptotic value based on Table 2. The
 511 **spectrum in (a) has been averaged for visualisation and hence has a lower resolution than the ‘raw’**
 512 **FFT (i.e., no averaging) used in BAYOMA.**

513 Here, the number of measured DOFs is $n = 5$ and the number of modes is $m = 2$. The dimension of
 514 the mode shape FIM $\mathbf{J}_{\Phi,\Phi}$ is then $mn = 10$. According to the theory, there are $m = 2$ zero
 515 eigenvalues of Type 0 (\mathcal{N}) due to norm constraint; $m(n - m) = 6$ eigenvalues of Type 1 (\mathcal{M}_\perp)
 516 comprising 2 possibly distinct eigenvalues each repeating $n - m = 3$ times; and $m(m - 1) = 2$
 517 eigenvalues of Type 2 (\mathcal{M}).

518 Figure 4(b) shows the eigenvalues of the mode shape FIM $\mathbf{J}_{\Phi,\Phi}$ based on (3) (circle, ‘exact’) and
 519 the high s/n asymptotic expression in Table 2 (cross, ‘asym.’). As the s/n ratio increases, the two sets
 520 of values converge to each other, verifying the asymptotic correctness of the latter. Each point of
 521 Type 1 in fact contains three visually overlapping points as the eigenvalues of this type repeat three
 522 times. The eigenvalues of Type 1 are greater than those of Type 2 by orders of magnitude and
 523 increase with s/n ratio because they grow with S_e^{-1} (see $J_{\Phi,\Phi}^{(1)}$ in Table 2). The magnitude of Type
 524 2 does not depend on S_e (see $J_{\Phi,\Phi}^{(2)}$ in Table 2). A direct implication of this is that Type 1
 525 uncertainty (orthogonal to MSS) will vanish with noiseless data while Type 2 uncertainty (within MSS)
 526 will still prevail.

527 Figure 5 shows the c.o.v. (coefficient of variation) of frequencies, damping ratios and mode shapes
 528 based on the exact (circle) and asymptotic FIM (cross). For the frequencies and damping ratios, the

529 c.o.v. is simply the ratio of posterior standard deviation to MPV. The mode shape c.o.v. is the square
 530 root sum of the eigenvalues of the $(n \times n)$ posterior mode shape covariance matrix. For small
 531 uncertainty it can be interpreted as the expected value of the hyper angle between the uncertain
 532 mode shape and the MPV. As seen in Figure 5, as the s/n ratio increases, the two values converge to
 533 each other, verifying the asymptotic correctness of the asymptotic FIM for high s/n ratio.



534

535 **Figure 5 Comparison of c.o.v. based on exact FIM (circle) and asymptotic FIM (cross)**

536 **10.2 Application to field data**

537 Consider a set of triaxial (x,y,z) ambient acceleration data of 36 hours at 50Hz measured on the roof
 538 of Tall building B in [4] during Typhoon Koppu (14 Sep. 2009); see Figure 6(a). Figure 1 shows the
 539 root PSD and root SV spectra of 30 minutes data before the main event. The two close modes
 540 around 0.18Hz are translational in nature. Their modal properties were identified (MPV and c.o.v.)
 541 previously by BAYOMA using the FFT in the band indicated. The theory in this work offers an
 542 opportunity for understanding their ID uncertainty especially in the mode shapes.

543 **10.2.1 Mode shape uncertainty from 30 minutes data**

544 We first investigate the ID uncertainty of mode shapes using the set of 30 minutes data. To give a
 545 basic idea of modal ID results (MPV, c.o.v.), the frequencies are identified to be 0.184 Hz (0.2%) and
 546 0.189 Hz (0.2%); the damping ratios are 0.54% (30%) and 0.92% (23%). The s/n ratio in terms of PSD
 547 at natural frequency is high, about a few thousands, which is also evidenced from Figure 1.

548 Given the 30 minutes data, the full posterior covariance matrix comprising all parameters is
 549 calculated. The 3×3 posterior covariance matrix of each mode shape is taken from the
 550 corresponding partition in the full covariance matrix. The results are shown in Table 5. The type
 551 indicated below each eigenvalue is determined based on the direction of the eigenvector. For Mode
 552 1, the eigenvalue $8.39e-7$ has a MAC of practically 1 with the most probable mode shape and so it

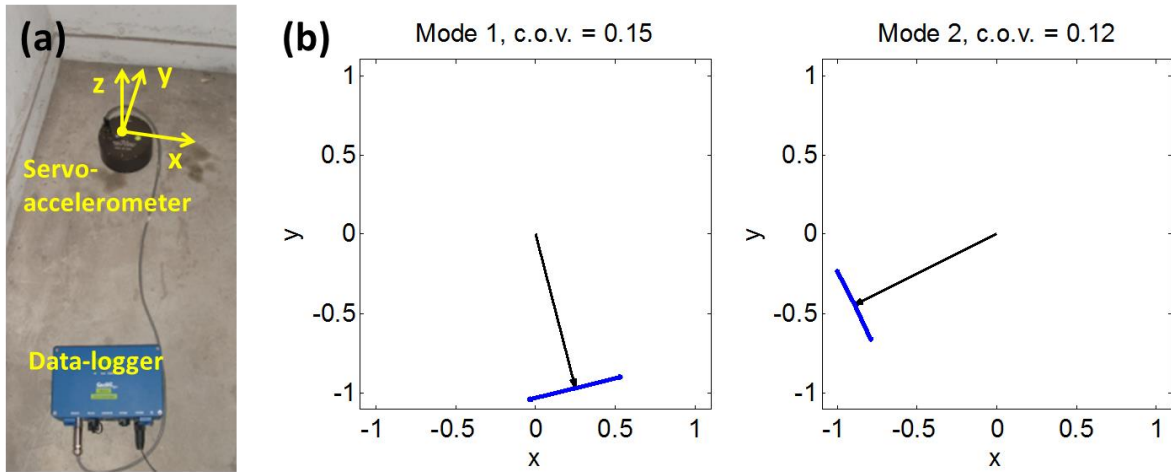
553 corresponds to Type 0 (norm-constrained). Its value is not exactly zero due to numerical errors,
554 which is typical. While the other two eigenvectors have a MAC of practically zero with the most
555 probable mode shape, the one with eigenvalue $8.21e-9$ is also orthogonal to Mode 2, and so it
556 corresponds to Type 1 (uncertainty orthogonal to MSS). This eigenvalue is not theoretically zero, but
557 is inversely proportional to the s/n ratio. It can be smaller than the calculated eigenvalue of Type 0
558 when the s/n ratio is high, as in the present case. The remaining eigenvector with eigenvalue $2.16e-2$
559 corresponds to Type 2 (uncertainty within MSS). Summing the eigenvalues and taking square root
560 gives a mode shape c.o.v. of 15%, which is clearly dominated by Type 2. Similar observations apply to
561 Mode 2, which has a c.o.v. of 12%. It should be noted that before this work the mode shape
562 covariance matrix can be calculated numerically but there is little or no insight on why such values
563 are obtained. Based on the theory in this work we are now able to understand why the results turn
564 out the way they appear. For example, there should be no surprise now why in Table 5 the largest
565 eigenvalue is several orders of magnitude larger than the second eigenvalue – it is of Type 2 that
566 does not diminish with the quality of data. Without the theory in this work one may wonder if this is
567 due to numerical error. The large disparity in Type 1 and 2 also suggests that one can simply focus on
568 Type 2 uncertainty, which is confined within the mode shape subspace with dimension often much
569 smaller than the whole space.

570 **Table 5 Eigenvalues of mode shape covariance matrix and mode shape c.o.v.**

Mode	Eigenvalues			c.o.v.
1	$8.21e-9$ (Type 1)	$8.39e-7$ (Type 0)	$2.16e-2$ (Type 2)	15%
2	$6.01e-9$ (Type 1)	$6.27e-7$ (Type 0)	$1.47e-2$ (Type 2)	12%

571

572 Figure 6(b) shows the most probable mode shapes with an arrow pointing from the origin. The two
573 mode shapes have a MAC of 0.21 and so they are not orthogonal. The blue arrows show the ‘ \pm two-
574 sigma’ uncertain mode shape deviation of the largest eigenvalue (Type 2), i.e., two times the term
575 $\sqrt{\delta_i} \mathbf{u}_i$ in (27). Only the xy view is shown because the mode shape component along the z direction
576 is negligible. The principal mode shape deviations are roughly tangential to the unit circle, which is
577 consistent with the fact that the mode shapes have unit length (in the unit sphere).

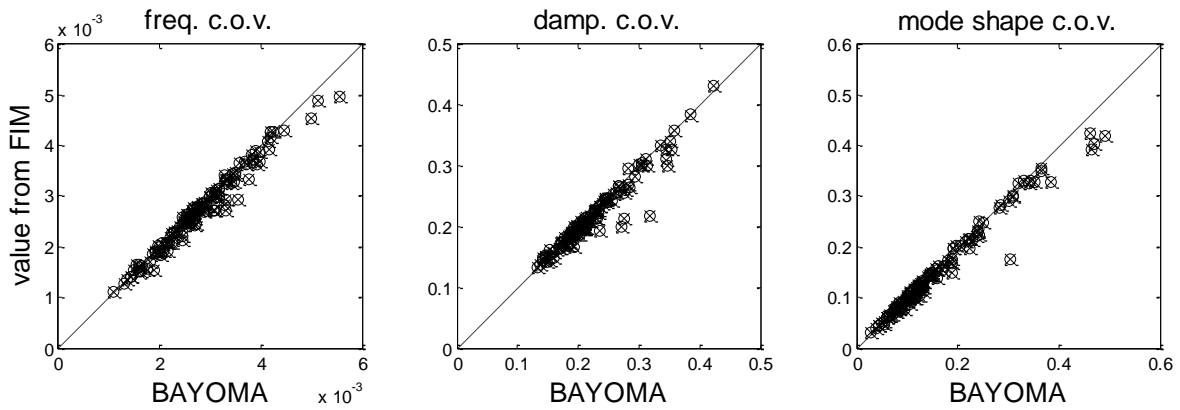


578

579 **Figure 6 (a) Sensor and data logger. (b) MPV of mode shapes (black, pointing from origin) and**
 580 **\pm two-sigma uncertainty (blue) of Type 2.**

581 **10.3 Comparison of c.o.v. from asymptotic FIM, exact FIM and BAYOMA**

582 We next compare the values of posterior c.o.v. based on the high s/n asymptotic FIM (Table 2), exact
 583 FIM (equation (3)) and BAYOMA ([22], for given data). For this purpose we divide the 36 hours data
 584 into non-overlapping windows of 30 minutes and identify the modal properties of the two modes
 585 (MPV and c.o.v.) using BAYOMA. The high s/n asymptotic FIM and exact FIM are then calculated
 586 using the MPV (the best one can do, since there is no ‘true’ value). The pseudo-inverse of these
 587 matrices (ignoring zero eigenvalues from norm constraints) gives the covariance matrix, from which
 588 the c.o.v. can be obtained. Figure 7 summarises the results (Modes 1 and 2 are not distinguished).
 589 The c.o.v. values of BAYOMA are plotted on the x-axis. The c.o.v. values from FIM are plotted on the
 590 y-axis, with the crosses for the high s/n asymptotic FIM and circles for the exact FIM. The crosses and
 591 circles almost overlap, which is consistent with the fact that the s/n ratio of data is quite high (at
 592 least a few thousands). The crosses and circles do not lie along the 1:1 dashed line, indicating a
 593 discrepancy between the c.o.v. from FIM and BAYOMA. This does not discredit the FIM or the high
 594 s/n asymptotic FIM, as the c.o.v. from BAYOMA is for a given data set and it always has a random
 595 part, though theoretically negligible for long data and assuming no modelling error and existence of
 596 ‘true’ parameter values. The discrepancy may reveal scenarios of modelling error, e.g., non-flat
 597 spectrum or non-classical damping, although there is little understanding about this aspect. More
 598 comparison and discussion about the meaning of ID uncertainty based on the exact FIM and
 599 BAYOMA can be found in [28]. Recognising that the x-axis is the uncertainty we can only calculate for
 600 given data (but no insight) and the y-axis (cross) is the uncertainty we can explain in the context of
 601 structural dynamics, the clustering of points around the 1:1 lines in Figure 7 represents an important
 602 progress in our understanding of ID uncertainty in close modes.



603

604 **Figure 7 Comparison of posterior c.o.v. from BAYOMA (for given data) and FIM. Cross ('x') – based**
 605 **on high s/n asymptotic FIM (Table 2), circle ('o') – based on exact FIM (3). Each point refers to the**
 606 **result of 30 minutes data out of 36 hours (so total 72 points).**

607 11 Conclusions

608 This work has performed an analytical study on the ID uncertainty of close modes that contributes to
 609 its understanding and provides a pathway for development of explicit formulae governing
 610 uncertainty, i.e., 'uncertainty law', in the future. The basic assumptions in the ID model include
 611 linear dynamics with classically damped modes, stationary modal excitations with constant PSD
 612 matrix within resonance band and stationary noise i.i.d. among measured DOFs with a constant PSD
 613 within the resonance band. Data is assumed to be sufficiently long in the sense that the number of
 614 FFT points in the resonance band is large compared to 1 (see Section 4); and has high s/n ratio (see
 615 (47)).

616 Before this work it was possible to calculate the posterior covariance matrix for given data using a
 617 Bayesian modal ID algorithm (BAYOMA) but it had not been possible to develop insights such as can
 618 be realised for well-separated modes. The large size of the matrix and its lack of sparseness, i.e., all
 619 parameters (except the noise PSD) are significantly correlated, has been identified as the cause. This
 620 work has discovered analytically the intrinsic correlation structure of the covariance matrix for long
 621 data and high s/n ratio, supported by mathematical proof, numerical verification and application
 622 with field data. The high s/n asymptotic expressions of Fisher Information Matrix (FIM, Table 2) and
 623 the analytical eigenvalue properties (Table 3) discovered are milestones for developing uncertainty
 624 laws for close modes that allow one to master the identification uncertainty and manage in ambient
 625 vibration tests. While the dimension of the posterior covariance matrix grows linearly with the
 626 number of measured DOFs, the theory in this work has reduced it to one independent of the number.
 627 The complexity w.r.t. the measured DOFs, which has been one of the major hurdles, has been
 628 resolved.

629 Mode shape uncertainty in well-separated modes is often negligible as it diminishes with increased
 630 data quality. This work has shown that the same is not true for close modes, where for each mode
 631 there is significant uncertainty within the mode shape subspace (MSS). Intuitively the mode shapes
 632 can ‘trade’ their directions within the MSS to give a similar likelihood value in Bayesian inference (or
 633 ‘data fit’ in non-Bayesian methods), and hence is less distinguishable. Such uncertainty does not
 634 diminish even for noiseless data. This puts a limit on the achievable precision of OMA with close
 635 modes. This mode shape uncertainty potentially correlates with all other parameters. Understanding
 636 such correlation structure requires yet another level of advance in the theory.

637 This work has not reached the ultimate goal of ‘uncertainty laws’, i.e., explicitly relating ID
 638 uncertainty to test configuration for understanding and test planning, but the analytical expressions
 639 of FIM (Table 2) and understanding about its eigenvalue properties (Table 3) shed light on possibility
 640 and provide the pathway to it. Obtaining the uncertainty laws will require further analytical
 641 investigation on the FIM and its inverse to produce explicit and manageable expressions for the
 642 posterior variances of modal properties – a big challenge, considering the large dimension of the FIM
 643 and entangling of modes.

644 **12 Acknowledgements**

645 This work is part of a research project on “Uncertainty quantification and management in ambient
 646 modal identification” funded by the Engineering and Physical Sciences Research Council (grant
 647 EP/N017897/1 and EP/N017803/1) to understand ID uncertainty and provide a strong scientific basis
 648 for implementing and planning ambient vibration tests. The research materials supporting this
 649 publication can be accessed by contacting ivanau@ntu.edu.sg.

650 **13 Appendix. Derivation of J_{xy} , J_{xS_e} and $J_{S_e S_e}$ ($x, y = f, \zeta, S$) in Table 2**

651 The expressions can be derived by substituting the Taylor expansion of \mathbf{E}_k^{-1} from (9) and the
 652 derivatives in (11) into (3), evaluating terms of increasing order and retaining the leading order term.

653 The expression of $J_{S_e S_e}$ is obtained by replacing \mathbf{E}_k^{-1} by its 0th order term, i.e., \mathbf{Q} , using

654 $\mathbf{E}_k^{(S_e)} = \mathbf{I}_m$ in (11) and noting that $tr(\mathbf{Q}\mathbf{Q}) = tr(\mathbf{Q}) = n - m$.

655 For J_{xy} , since \mathbf{E}_k^{-1} appears twice in (3), the 0th order of J_{xy} involves the 0th × 0th order of \mathbf{E}_k^{-1} .

656 Since the 0th order of \mathbf{E}_k^{-1} is \mathbf{Q} and $\mathbf{Q}\bar{\Phi} = \bar{\Phi}^T \mathbf{Q} = \mathbf{0}$, the 0th order of J_{xy} is zero. The 1st order of

657 J_{xy} involves the $0^{\text{th}} \times 1^{\text{st}}$ order + $1^{\text{st}} \times 0^{\text{th}}$ order of \mathbf{E}_k^{-1} . For the same reason as before, these terms
658 are zero. The 2^{nd} order of J_{xy} involves the $0^{\text{th}} \times 2^{\text{nd}} + 1^{\text{st}} \times 1^{\text{st}}$ order of \mathbf{E}_k^{-1} . The former is zero. The
659 latter is not zero and hence is the leading order of J_{xy} as given in Table 2. To obtain the expression,
660 note that

$$661 \quad (1^{\text{st}} \text{ order of } \mathbf{E}_k^{-1}) \times \mathbf{E}_k^{(x)} = (S_e^{-1} \mathbf{R}^T \boldsymbol{\varepsilon}_k \mathbf{R}) (\overline{\Phi} \mathbf{H}_k^{(x)} \overline{\Phi}^T) = \mathbf{R}^T \mathbf{H}_k^{-1} \mathbf{H}_k^{(x)} \overline{\Phi}^T \quad (29)$$

662 since $\mathbf{R} \overline{\Phi} = \mathbf{I}_m$ and $\boldsymbol{\varepsilon}_k = S_e \mathbf{H}_k^{-1}$. This gives the expression in Table 2:

$$663 \quad J_{xy} \sim \text{tr} \Sigma (\mathbf{R}^T \mathbf{H}_k^{-1} \mathbf{H}_k^{(x)} \overline{\Phi}^T) (\mathbf{R}^T \mathbf{H}_k^{-1} \mathbf{H}_k^{(y)} \overline{\Phi}^T) = \text{tr} \Sigma \mathbf{H}_k^{-1} \mathbf{H}_k^{(x)} \mathbf{H}_k^{-1} \mathbf{H}_k^{(y)} \quad (30)$$

664 where we have used the cyclic property of trace ($\text{tr}(AB) = \text{tr}(BA)$) to move the $\overline{\Phi}^T$ on the right
665 end to the left end and then $\overline{\Phi}^T \mathbf{R}^T = (\mathbf{R} \overline{\Phi})^T = \mathbf{I}_m$ to simplify.

666 Applying the same argument above to J_{xS_e} shows that its leading order is also the $1^{\text{st}} \times 1^{\text{st}}$ order of
667 \mathbf{E}_k^{-1} . Using (29),

$$668 \quad J_{xS_e} \sim \text{tr} \Sigma (\mathbf{R}^T \mathbf{H}_k^{-1} \mathbf{H}_k^{(x)} \overline{\Phi}^T) (S_e^{-1} \mathbf{R}^T \boldsymbol{\varepsilon}_k \mathbf{R}) = \text{tr} \Sigma (\overline{\Phi}^T \overline{\Phi})^{-1} \mathbf{H}_k^{-1} \mathbf{H}_k^{(x)} \mathbf{H}_k^{-1} \quad (31)$$

669 where we have used the cyclic property of trace to move the \mathbf{R} on the right end to the left end;
670 then $\mathbf{R} \mathbf{R}^T = (\overline{\Phi}^T \overline{\Phi})^{-1}$, $\overline{\Phi}^T \mathbf{R}^T = \mathbf{I}_m$ and $\boldsymbol{\varepsilon}_k = S_e \mathbf{H}_k^{-1}$ to simplify.

671 **14 Appendix. Derivation of (13), (14) and (15) in Section 6**

672 Substituting (11) and (12) into (3) gives

$$673 \quad J_{x\Phi_{ri}} = \text{tr} \Sigma \mathbf{E}_k^{-1} (\overline{\Phi} \mathbf{H}_k^{(x)} \overline{\Phi}^T) \mathbf{E}_k^{-1} (\overline{\Phi}^{(\Phi_{ri})} \mathbf{H}_k \overline{\Phi}^T + \overline{\Phi} \mathbf{H}_k \overline{\Phi}^{(\Phi_{ri})T}) \quad x = f, \zeta, \mathbf{S} \quad (32)$$

$$674 \quad J_{S_e \Phi_{ri}} = \text{tr} \Sigma \mathbf{E}_k^{-2} (\overline{\Phi}^{(\Phi_{ri})} \mathbf{H}_k \overline{\Phi}^T + \overline{\Phi} \mathbf{H}_k \overline{\Phi}^{(\Phi_{ri})}) \quad (33)$$

$$675 \quad J_{xy} = \text{tr} \Sigma \mathbf{E}_k^{-1} (\overline{\Phi}^{(x)} \mathbf{H}_k \overline{\Phi}^T + \overline{\Phi} \mathbf{H}_k \overline{\Phi}^{(x)T}) \mathbf{E}_k^{-1} (\overline{\Phi}^{(y)} \mathbf{H}_k \overline{\Phi}^T + \overline{\Phi} \mathbf{H}_k \overline{\Phi}^{(y)T}) \quad x, y = \Phi \quad (34)$$

676 Using (56) and (57) in Section 16 (appendix) to simplify gives

677 $J_{x\Phi_{ri}} = 2 \text{Re tr} \Sigma \mathbf{E}_k^{-1} \overline{\Phi} \mathbf{H}_k^{(x)} \overline{\Phi}^T \mathbf{E}_k^{-1} \overline{\Phi}^{(\Phi_{ri})} \mathbf{H}_k \overline{\Phi}^T \quad x = f, \zeta, \mathbf{S} \quad (35)$

678 $J_{S_e \Phi_{ri}} = 2 \text{Re tr} \Sigma \mathbf{E}_k^{-2} \overline{\Phi}^{(\Phi_{ij})} \mathbf{H}_k \overline{\Phi}^T \quad (36)$

679 $J_{xy} = 2 \text{Re tr} \Sigma \mathbf{E}_k^{-1} \overline{\Phi}^{(x)} \mathbf{H}_k \overline{\Phi}^T \mathbf{E}_k^{-1} (\overline{\Phi}^{(y)} \mathbf{H}_k \overline{\Phi}^T + \overline{\Phi} \mathbf{H}_k \overline{\Phi}^{(y)T}) \quad x, y = \Phi \quad (37)$

680 Substituting the Taylor expansion of \mathbf{E}_k^{-1} from (9) and taking the leading order term gives (13) to
681 (15). Details are presented separately in Sections 14.1 to 14.3 below.

682 **14.1 $J_{x\Phi_{ri}}$ in (13) for $x = f, \zeta, \mathbf{S}$**

683 Substituting (9) into (35) gives the following terms of different orders:

684 0th order of $J_{x\Phi_{ri}}$ involves 0th x 0th order of \mathbf{E}_k^{-1}

685 1st order of $J_{x\Phi_{ri}}$ involves 0th x 1st + 1st x 0th order of \mathbf{E}_k^{-1}

686 2nd order of $J_{x\Phi_{ri}}$ involves 0th x 2nd + 2nd x 0th + 1st x 1st order of \mathbf{E}_k^{-1}

687 Due to the property of \mathbf{Q} , any product involving the 0th order of \mathbf{E}_k^{-1} gives zero. This implies that
688 the 0th and 1st order of $J_{x\Phi_{ri}}$ is zero. The leading order of $J_{x\Phi_{ri}}$ is then the second order term
689 involving the 1st x 1st order of \mathbf{E}_k^{-1} . Evaluating it gives the expression in (13):

690
$$J_{x\Phi_{ri}} \sim 2S_e^{-2} \text{Re tr} \Sigma (\mathbf{R}^T \boldsymbol{\varepsilon}_k \mathbf{R}) (\overline{\Phi} \mathbf{H}_k^{(x)} \overline{\Phi}^T) (\mathbf{R}^T \boldsymbol{\varepsilon}_k \mathbf{R}) (\overline{\Phi}^{(\Phi_{ri})} \mathbf{H}_k \overline{\Phi}^T) \quad (38)$$

$$= 2 \text{Re tr} \Sigma [\mathbf{H}_k^{(x)} \mathbf{H}_k^{-1} \mathbf{R} \overline{\Phi}^{(\Phi_{ri})}]$$

691 where we have used the cyclic property of trace to move $\mathbf{H}_k \overline{\Phi}^T$ on the right end to the left end;
692 then $\overline{\Phi}^T \mathbf{R}^T = \mathbf{I}_m$ and $\boldsymbol{\varepsilon}_k = S_e \mathbf{H}_k^{-1}$ to simplify.

693 **14.2 $J_{S_e \Phi_{ri}}$ in (14)**

694 Using \mathbf{E}_k^{-1} from (9) and expanding the square of $\mathbf{E}_k^{-2} = (\mathbf{E}_k^{-1})^2$ gives terms of different order. The
695 0th order of \mathbf{E}_k^{-2} is $S_e^{-2} \mathbf{Q}$ because $\mathbf{Q}^2 = \mathbf{Q}$. Replacing \mathbf{E}_k^{-2} in (36) by $S_e^{-2} \mathbf{Q}$ and using the cyclic
696 property of trace and $\overline{\Phi}^T \mathbf{Q} = \mathbf{0}$ gives a zero vector. The leading order of $J_{S_e \Phi_{ri}}$ should then come
697 from the higher order terms of \mathbf{E}_k^{-2} . The 1st order of \mathbf{E}_k^{-2} comes from the 0th x 1st and 1st x 0th order
698 term of \mathbf{E}_k^{-1} . Using $\mathbf{Q} \overline{\Phi} = \overline{\Phi}^T \mathbf{Q} = \mathbf{0}$ shows that they are all zero. The next higher order term of
699 \mathbf{E}_k^{-2} is the 2nd order given by the 1st x 1st order term of \mathbf{E}_k^{-1} :

700 $\mathbf{E}_k^{-2} \sim S_e^{-2} (\mathbf{R}^T \boldsymbol{\varepsilon}_k \mathbf{R})(\mathbf{R}^T \boldsymbol{\varepsilon}_k \mathbf{R}) = S_e^{-2} \mathbf{R}^T \boldsymbol{\varepsilon}_k (\overline{\boldsymbol{\Phi}}^T \overline{\boldsymbol{\Phi}})^{-1} \boldsymbol{\varepsilon}_k \mathbf{R}$ (39)

701 since $\mathbf{R} \mathbf{R}^T = (\overline{\boldsymbol{\Phi}}^T \overline{\boldsymbol{\Phi}})^{-1}$. Substituting into (36) gives

702 $J_{S_e \Phi_{ri}} \sim 2S_e^{-2} \text{Re tr} \Sigma [\mathbf{R}^T \boldsymbol{\varepsilon}_k (\overline{\boldsymbol{\Phi}}^T \overline{\boldsymbol{\Phi}})^{-1} \boldsymbol{\varepsilon}_k \mathbf{R} \overline{\boldsymbol{\Phi}}^{(\Phi_{ri})} \mathbf{H}_k \overline{\boldsymbol{\Phi}}^T]$
 703 $= 2 \text{Re tr} \Sigma [(\overline{\boldsymbol{\Phi}}^T \overline{\boldsymbol{\Phi}})^{-1} \mathbf{H}_k^{-1} \mathbf{R} \overline{\boldsymbol{\Phi}}^{(\Phi_{ri})}]$ (40)

703 where we have used the cyclic property of trace to move $\mathbf{H}_k \overline{\boldsymbol{\Phi}}^T$ on the right end to the left end;

704 then $\overline{\boldsymbol{\Phi}}^T \mathbf{R}^T = \mathbf{I}_m$ and $\boldsymbol{\varepsilon}_k = S_e \mathbf{H}_k^{-1}$ to simplify.

705 14.3 J_{xy} in (15) for $x, y = \Phi$

706 Substituting (9) into (37) gives the 0th, 1st and 2nd order terms of J_{xy} , which are denoted by $J_{xy}^{(0)}$,

707 $J_{xy}^{(1)}$ and $J_{xy}^{(2)}$, respectively. The 0th order $J_{xy}^{(0)}$ involves the 0th x 0th order of \mathbf{E}_k^{-1} . Replacing \mathbf{E}_k^{-1}

708 by its 0th order \mathbf{Q} and expanding gives

709 $J_{xy}^{(0)} = 2S_e^{-2} \text{Re tr} \Sigma [\mathbf{Q} \overline{\boldsymbol{\Phi}}^{(x)} \mathbf{H}_k \overline{\boldsymbol{\Phi}}^T \mathbf{Q} \overline{\boldsymbol{\Phi}}^{(y)} \mathbf{H}_k \overline{\boldsymbol{\Phi}}^T + \mathbf{Q} \overline{\boldsymbol{\Phi}}^{(x)} \mathbf{H}_k \overline{\boldsymbol{\Phi}}^T \mathbf{Q} \overline{\boldsymbol{\Phi}} \mathbf{H}_k \overline{\boldsymbol{\Phi}}^{(y)T}] = 0$ (41)

710 because the trace of both terms are zero: for the first term, use the cyclic property of trace to move

711 $\overline{\boldsymbol{\Phi}}^T$ on the right end to the left end and find $\overline{\boldsymbol{\Phi}}^T \mathbf{Q} = \mathbf{0}$; the second term has $\mathbf{Q} \overline{\boldsymbol{\Phi}} = \mathbf{0}$.

712 Next, $J_{xy}^{(1)}$ involves the 0th x 1st + 1st x 0th order of \mathbf{E}_k^{-1} . The latter can be seen to be zero after using

713 $\overline{\boldsymbol{\Phi}}^T \mathbf{Q} = \mathbf{0}$. Thus $J_{xy}^{(1)}$ only involves the 0th x 1st order of \mathbf{E}_k^{-1} :

714 $J_{xy}^{(1)} = 2S_e^{-2} \text{Re tr} \Sigma [\mathbf{Q} \overline{\boldsymbol{\Phi}}^{(x)} \mathbf{H}_k \overline{\boldsymbol{\Phi}}^T (\mathbf{R}^T \boldsymbol{\varepsilon}_k \mathbf{R})(\overline{\boldsymbol{\Phi}}^{(y)} \mathbf{H}_k \overline{\boldsymbol{\Phi}}^T + \overline{\boldsymbol{\Phi}} \mathbf{H}_k \overline{\boldsymbol{\Phi}}^{(y)T})]$
 715 $= 2S_e^{-1} \text{Re tr} \Sigma [\mathbf{Q} \overline{\boldsymbol{\Phi}}^{(x)} \mathbf{R}(\overline{\boldsymbol{\Phi}}^{(y)} \mathbf{H}_k \overline{\boldsymbol{\Phi}}^T + \overline{\boldsymbol{\Phi}} \mathbf{H}_k \overline{\boldsymbol{\Phi}}^{(y)T})]$ (42)

715 after using $\overline{\boldsymbol{\Phi}}^T \mathbf{R}^T = \mathbf{I}_m$ and $\boldsymbol{\varepsilon}_k = S_e \mathbf{H}_k^{-1}$. Multiplying gives two terms. For the first term, use the

716 cyclic property of trace to move $\overline{\boldsymbol{\Phi}}^T$ on the right end to the left end; then use $\overline{\boldsymbol{\Phi}}^T \mathbf{Q} = \mathbf{0}$ to see

717 that the first term is zero. This leaves the second term as the expression in (16):

718 $J_{xy}^{(1)} \sim 2S_e^{-1} \text{Re tr} \Sigma [\mathbf{Q} \overline{\boldsymbol{\Phi}}^{(x)} \mathbf{R} \overline{\boldsymbol{\Phi}} \mathbf{H}_k \overline{\boldsymbol{\Phi}}^{(y)T}] = 2S_e^{-1} \text{tr} [\mathbf{Q} \overline{\boldsymbol{\Phi}}^{(x)} (\text{Re} \Sigma \mathbf{H}_k) \overline{\boldsymbol{\Phi}}^{(y)T}]$ (43)

719 after using $\mathbf{R} \overline{\boldsymbol{\Phi}} = \mathbf{I}_m$ and carrying $\text{Re} \Sigma$ inside.

720 Finally, $J_{xy}^{(2)}$ involves the 0th x 2nd + 1st x 1st + 2nd x 0th of \mathbf{E}_k^{-1} . Substituting into (37) and simplifying

721 shows that the 2nd x 0th term is zero. Using similar arguments as before,

0th x 2nd term

$$\begin{aligned}
&= -2S_e^{-2} \text{Re tr} \Sigma [\mathbf{Q}(\overline{\Phi}^{(x)} \mathbf{H}_k \overline{\Phi}^T) (\mathbf{R}^T \boldsymbol{\varepsilon}_k (\overline{\Phi}^T \overline{\Phi})^{-1} \boldsymbol{\varepsilon}_k \mathbf{R}) (\overline{\Phi}^{(y)} \mathbf{H}_k \overline{\Phi}^T + \overline{\Phi} \mathbf{H}_k \overline{\Phi}^{(y)T})] \\
722 \quad &= -2S_e^{-1} \text{Re tr} \Sigma [\mathbf{Q} \overline{\Phi}^{(x)} (\overline{\Phi}^T \overline{\Phi})^{-1} \boldsymbol{\varepsilon}_k \mathbf{R} (\overline{\Phi}^{(y)} \mathbf{H}_k \overline{\Phi}^T + \overline{\Phi} \mathbf{H}_k \overline{\Phi}^{(y)T})] \\
&= -2N_f \text{tr} [\mathbf{Q} \overline{\Phi}^{(x)} (\overline{\Phi}^T \overline{\Phi})^{-1} \overline{\Phi}^{(y)T}]
\end{aligned} \tag{44}$$

723 where the trace of the first term in the second equality is zero;

1st x 1st term

$$\begin{aligned}
&= 2S_e^{-2} \text{Re tr} \Sigma (\mathbf{R}^T \boldsymbol{\varepsilon}_k \mathbf{R}) (\overline{\Phi}^{(x)} \mathbf{H}_k \overline{\Phi}^T) (\mathbf{R}^T \boldsymbol{\varepsilon}_k \mathbf{R}) (\overline{\Phi}^{(y)} \mathbf{H}_k \overline{\Phi}^T + \overline{\Phi} \mathbf{H}_k \overline{\Phi}^{(y)T}) \\
724 \quad &= 2S_e^{-1} \text{Re tr} \Sigma [\mathbf{R}^T \boldsymbol{\varepsilon}_k \mathbf{R} \overline{\Phi}^{(x)} \mathbf{R} (\overline{\Phi}^{(y)} \mathbf{H}_k \overline{\Phi}^T + \overline{\Phi} \mathbf{H}_k \overline{\Phi}^{(y)T})] \\
&= 2N_f \text{tr} [\mathbf{R} \overline{\Phi}^{(x)} \mathbf{R} \overline{\Phi}^{(y)}] + 2 \text{Re tr} \Sigma [\mathbf{R}^T \mathbf{H}_k^{-1} \mathbf{R} \overline{\Phi}^{(x)} \mathbf{H}_k \overline{\Phi}^{(y)T}]
\end{aligned} \tag{45}$$

725 after expanding and using the cyclic property of trace. Combining (44) and (45),

$$\begin{aligned}
726 \quad J_{xy}^{(2)} &= -2N_f \text{tr} [\mathbf{Q} \overline{\Phi}^{(x)} (\overline{\Phi}^T \overline{\Phi})^{-1} \overline{\Phi}^{(y)T}] \\
&\quad + 2N_f \text{tr} [\mathbf{R} \overline{\Phi}^{(x)} \mathbf{R} \overline{\Phi}^{(y)}] + 2 \text{Re tr} \Sigma [\mathbf{R}^T \mathbf{H}_k^{-1} \mathbf{R} \overline{\Phi}^{(x)} \mathbf{H}_k \overline{\Phi}^{(y)T}]
\end{aligned} \tag{46}$$

727 Note that $J_{xy}^{(1)}$ in (43) and the first term in (46) both contain $\mathbf{Q} \overline{\Phi}^{(x)}$ on the left and $\overline{\Phi}^{(y)T}$ on the
728 right. Assume that the modes are ‘sufficiently linearly independent’ in the sense that (e.g., in terms
729 of eigenvalues)

$$730 \quad S_e (N_f^{-1} \text{Re} \Sigma \mathbf{H}_k)^{-1} (\overline{\Phi}^T \overline{\Phi})^{-1} \ll \mathbf{I}_m \tag{47}$$

731 In this case the first term in (46) is negligible compared to $J_{xy}^{(1)}$. Omitting it gives (17).

732 **15 Appendix. Derivation of $J_{x\phi_i}$, $J_{S_e\phi_i}$ and $J_{\Phi:\Phi}$ in Table 2**

733 **15.1 $J_{x\phi_i}$ and $J_{S_e\phi_i}$**

734 The steps for deriving $J_{x\phi_i}$ and $J_{S_e\phi_i}$ are the same so here we consider $J_{x\phi_i}$ only. Substituting
735 (18) with $\|\boldsymbol{\phi}_i\| = 1$ into (13) and carrying the summation inside,

$$736 \quad J_{x\phi_{ri}} \sim 2 \text{tr} [(\text{Re} \Sigma \mathbf{H}_k^{(x)} \mathbf{H}_k^{-1}) \mathbf{R} (\mathbf{I}_n - \overline{\boldsymbol{\phi}}_i \overline{\boldsymbol{\phi}}_i^T) \mathbf{e}_r \mathbf{e}_i^T] \tag{48}$$

737 Using the cyclic property of trace to move \mathbf{e}_i^T to the left end so that the product inside $\text{tr}(\cdot)$
738 becomes a scalar, we obtain

$$739 \quad J_{x\phi_{ri}} \sim 2 \mathbf{e}_i^T (\text{Re} \Sigma \mathbf{H}_k^{(x)} \mathbf{H}_k^{-1}) \mathbf{R} (\mathbf{I}_n - \overline{\boldsymbol{\phi}}_i \overline{\boldsymbol{\phi}}_i^T) \mathbf{e}_r \tag{49}$$

740 Assembling $J_{x\Phi_i} = [J_{x\Phi_{1i}}, \dots, J_{x\Phi_{ni}}]$ and noting $[\mathbf{e}_1, \dots, \mathbf{e}_n] = \mathbf{I}_n$ and $\mathbf{R}(\mathbf{I}_n - \bar{\boldsymbol{\Phi}}_i \bar{\boldsymbol{\Phi}}_i^T) = \mathbf{Q}_i$ gives
741 the expression in Table 2.

742 **15.2 $J_{\boldsymbol{\Phi}, \boldsymbol{\Phi}}^{(1)}$ in Table 2**

743 Consider $J_{\Phi_{ri}\Phi_{sj}}^{(1)}$, i.e., J_{xy} in (16) with $x = \Phi_{ri}$ and $y = \Phi_{sj}$:

$$744 \quad J_{\Phi_{ri}\Phi_{sj}}^{(1)} \sim 2S_e^{-1} \text{tr}[\mathbf{Q}\bar{\boldsymbol{\Phi}}^{(\Phi_{ri})}(\text{Re}\Sigma\mathbf{H}_k)\bar{\boldsymbol{\Phi}}^{(\Phi_{sj})T}] \quad (50)$$

745 Using (58) in Section 16 (appendix) with $A = \mathbf{Q}$ and $B = \mathbf{H}_k$, and noting $\mathbf{Q}(\mathbf{I}_n - \bar{\boldsymbol{\Phi}}_j \bar{\boldsymbol{\Phi}}_j^T) = \mathbf{Q}$,

$$746 \quad J_{\Phi_{ri}\Phi_{sj}}^{(1)} \sim 2S_e^{-1} \mathbf{Q}(r, s) \text{Re}\Sigma\mathbf{H}_k(i, j) \quad (51)$$

747 where $\mathbf{Q}(r, s)$ denotes the (r, s) -entry of \mathbf{Q} ; similar notation for $\mathbf{H}_k(i, j)$. Assembling $J_{\Phi_{ri}\Phi_{sj}}^{(1)}$

748 for r and s from 1 to n into a matrix gives the (i, j) -partition of $J_{\boldsymbol{\Phi}, \boldsymbol{\Phi}}^{(1)}$:

$$749 \quad J_{\boldsymbol{\Phi}_i \boldsymbol{\Phi}_j}^{(1)} = 2S_e^{-1} [\text{Re}\Sigma\mathbf{H}_k(i, j)] \mathbf{Q} \quad (52)$$

750 Further assembling the partitions for i and j from 1 to m gives the expression in Table 2.

751 **15.3 $J_{\boldsymbol{\Phi}, \boldsymbol{\Phi}}^{(2)}$ in Table 2**

752 Using (18) to obtain $\bar{\boldsymbol{\Phi}}^{(\Phi_{ri})}$ and $\bar{\boldsymbol{\Phi}}^{(\Phi_{sj})}$ and substituting into (17),

1st term of $J_{\Phi_{ri}\Phi_{sj}}^{(2)}$

$$753 \quad \begin{aligned} &= 2N_f \text{tr}[\mathbf{R}(\mathbf{I}_n - \bar{\boldsymbol{\Phi}}_i \bar{\boldsymbol{\Phi}}_i^T) \mathbf{e}_r \mathbf{e}_i^T \mathbf{R}(\mathbf{I}_n - \bar{\boldsymbol{\Phi}}_j \bar{\boldsymbol{\Phi}}_j^T) \mathbf{e}_s \mathbf{e}_j^T] \\ &= 2N_f \text{tr}[\mathbf{Q}_i \mathbf{e}_r \mathbf{e}_i^T \mathbf{Q}_j \mathbf{e}_s \mathbf{e}_j^T] = 2N_f \text{tr}[\mathbf{e}_j^T \mathbf{Q}_j \mathbf{e}_r \mathbf{e}_i^T \mathbf{Q}_i \mathbf{e}_s] = 2N_f \text{tr}[\mathbf{e}_r^T \mathbf{Q}_i^T \mathbf{e}_j \mathbf{e}_i^T \mathbf{Q}_j \mathbf{e}_s] \end{aligned} \quad (53)$$

754 where the second equality has used the definition of \mathbf{Q}_i in (5). Similarly,

2nd term of $J_{\Phi_{ri}\Phi_{sj}}^{(2)}$

$$755 \quad \begin{aligned} &= 2 \text{Re} \text{tr} \Sigma [\mathbf{R}^T \mathbf{H}_k^{-1} \mathbf{R}(\mathbf{I}_n - \bar{\boldsymbol{\Phi}}_i \bar{\boldsymbol{\Phi}}_i^T) \mathbf{e}_r \mathbf{e}_i^T \mathbf{H}_k \mathbf{e}_j \mathbf{e}_s^T (\mathbf{I}_n - \bar{\boldsymbol{\Phi}}_j \bar{\boldsymbol{\Phi}}_j^T)] \\ &= 2 \text{Re} \text{tr} \Sigma [\mathbf{e}_s^T (\mathbf{I}_n - \bar{\boldsymbol{\Phi}}_j \bar{\boldsymbol{\Phi}}_j^T) \mathbf{R}^T \mathbf{H}_k^{-1} \mathbf{R}(\mathbf{I}_n - \bar{\boldsymbol{\Phi}}_i \bar{\boldsymbol{\Phi}}_i^T) \mathbf{e}_r \mathbf{e}_i^T \mathbf{H}_k \mathbf{e}_j] \\ &= 2 \text{Re} \text{tr} \Sigma [\mathbf{e}_s^T \mathbf{Q}_j^T \mathbf{H}_k^{-1} \mathbf{Q}_i \mathbf{e}_r \mathbf{e}_i^T \mathbf{H}_k \mathbf{e}_j] = 2 \text{Re} \Sigma \{ [\mathbf{Q}_j^T \mathbf{H}_k^{-1} \mathbf{Q}_i]_{(s,r)} \mathbf{H}_k(i, j) \} \\ &= 2 \text{Re} \Sigma \{ \mathbf{H}_k(i, j) [\mathbf{Q}_i^T \mathbf{H}_k^{-1} \mathbf{Q}_j]_{(r,s)} \} \end{aligned} \quad (54)$$

756 Combining (53) and (54) and assembling in matrix form for r and s from 1 to n ,

$$\begin{aligned}
757 \quad J_{\Phi_i \Phi_j}^{(2)} &= 2N_f \mathbf{Q}_i^T \mathbf{e}_j \mathbf{e}_i^T \mathbf{Q}_j + 2\text{Re}\Sigma\{\mathbf{H}_k(i, j) \mathbf{Q}_i^T \mathbf{H}_k^{-T} \mathbf{Q}_j\} \\
&= 2\mathbf{Q}_i^T [N_f \mathbf{e}_j \mathbf{e}_i^T + \text{Re}\Sigma \mathbf{H}_k(i, j) \mathbf{H}_k^{-T}] \mathbf{Q}_j
\end{aligned} \tag{55}$$

758 Further assembling the partitions for i and j from 1 to m gives the expression in Table 2.

759 **16 Appendix. Some useful identities**

760 For any complex matrix A and Hermitian X ,

$$761 \quad \text{tr}[X(A + A^*)] = 2\text{Re}\text{tr}(XA) \tag{56}$$

$$762 \quad \text{tr}[X(A + A^*)X(B + B^*)] = 2\text{Re}\text{tr}[XBX(A + A^*)] = 2\text{Re}\text{tr}[XAX(B + B^*)] \tag{57}$$

763 For any A ($n \times n$ complex) and B ($m \times m$ complex),

$$764 \quad \text{tr}[A \overline{\Phi}^{(\Phi_{ri})} B \overline{\Phi}^{(\Phi_{sj})T}] = \|\Phi_i\|^{-1} \|\Phi_j\|^{-1} [(\mathbf{I}_n - \overline{\Phi}_i \overline{\Phi}_i^T) A^T (\mathbf{I}_n - \overline{\Phi}_j \overline{\Phi}_j^T)]_{(r,s)} B(i, j) \tag{58}$$

765 Equation (56) was used to simplify (32) and (33). It can be shown as follow:

$$766 \quad \text{tr}[X(A + A^*)] = \text{tr}(XA) + \text{tr}(XA^*) = \text{tr}(XA) + \text{tr}(A^* X^*) = \text{tr}[XA + (XA)^*] = 2\text{Re}\text{tr}(XA) \tag{59}$$

767 where we have used $\text{tr}(XA^*) = \text{tr}(A^* X)$ (cyclic property of trace) and $X = X^*$ (Hermitian) in
768 arriving at the second and third equality, respectively.

769 Equation (57) was used to simplify (34). It can be shown by noting that $X(A + A^*)X^*$ is Hermitian
770 and applying (56):

$$771 \quad \text{tr}[X(A + A^*)X(B + B^*)] = 2\text{Re}\text{tr}[X(A + A^*)XB] = 2\text{Re}\text{tr}[XBX(A + A^*)] \tag{60}$$

772 after using the cyclic property of trace. Swapping A and B and using the cyclic property of trace
773 gives the other equality in (57).

774 Equation (58) was used to simplify (50). It can be shown as follow. Using (18) for $\overline{\Phi}^{(\Phi_{ri})}$ and
775 $\overline{\Phi}^{(\Phi_{sj})}$,

$$\begin{aligned}
&\text{tr}[A \overline{\Phi}^{(\Phi_{ri})} B \overline{\Phi}^{(\Phi_{sj})T}] \\
776 \quad &= \|\Phi_i\|^{-1} \|\Phi_j\|^{-1} \text{tr}[A(\mathbf{I}_n - \overline{\Phi}_i \overline{\Phi}_i^T) \mathbf{e}_r \mathbf{e}_i^T B \mathbf{e}_j \mathbf{e}_s^T (\mathbf{I}_n - \overline{\Phi}_j \overline{\Phi}_j^T)] \\
&= \|\Phi_i\|^{-1} \|\Phi_j\|^{-1} \text{tr}[A(\mathbf{I}_n - \overline{\Phi}_i \overline{\Phi}_i^T) \mathbf{e}_r \mathbf{e}_s^T (\mathbf{I}_n - \overline{\Phi}_j \overline{\Phi}_j^T)] B(i, j)
\end{aligned} \tag{61}$$

777 since $\mathbf{e}_i^T \mathbf{B} \mathbf{e}_j = B(i, j)$, i.e., the (i, j) -entry. Using the cyclic property of trace to move

778 $\mathbf{e}_s^T (\mathbf{I}_n - \bar{\boldsymbol{\varphi}}_j \bar{\boldsymbol{\varphi}}_j^T)$ to the left,

$$\begin{aligned}
 & tr[A \bar{\boldsymbol{\Phi}}^{(\Phi_{ri})} B \bar{\boldsymbol{\Phi}}^{(\Phi_{sj})T}] \\
 779 & = \|\boldsymbol{\varphi}_i\|^{-1} \|\boldsymbol{\varphi}_j\|^{-1} tr[\mathbf{e}_s^T (\mathbf{I}_n - \bar{\boldsymbol{\varphi}}_j \bar{\boldsymbol{\varphi}}_j^T) A (\mathbf{I}_n - \bar{\boldsymbol{\varphi}}_i \bar{\boldsymbol{\varphi}}_i^T) \mathbf{e}_r] B(i, j) \\
 & = \|\boldsymbol{\varphi}_i\|^{-1} \|\boldsymbol{\varphi}_j\|^{-1} [(\mathbf{I}_n - \bar{\boldsymbol{\varphi}}_j \bar{\boldsymbol{\varphi}}_j^T) A (\mathbf{I}_n - \bar{\boldsymbol{\varphi}}_i \bar{\boldsymbol{\varphi}}_i^T)]_{(s,r)} B(i, j) \\
 & = \|\boldsymbol{\varphi}_i\|^{-1} \|\boldsymbol{\varphi}_j\|^{-1} [(\mathbf{I}_n - \bar{\boldsymbol{\varphi}}_i \bar{\boldsymbol{\varphi}}_i^T) A^T (\mathbf{I}_n - \bar{\boldsymbol{\varphi}}_j \bar{\boldsymbol{\varphi}}_j^T)]_{(r,s)} B(i, j)
 \end{aligned} \tag{62}$$

780 17 References

- 781 [1] N.M.M Maia, J.M.M Silva, Theoretical and Experimental Modal Analysis, Research Studies Press
 782 Ltd, Somerset, England, 1997.
- 783 [2] D.J. Ewins, Modal testing: Theory and practice, Research Studies Press, PA, USA, 2000.
- 784 [3] F.N. Catbas, T. Kijewski-Correa, A.E. Aktan (eds), Structural Identification of Constructed Systems:
 785 Approaches, Methods, and Technologies for Effective Practice of St-Id, American Society of Civil
 786 Engineers, 2011.
- 787 [4] S.K. Au, F.L. Zhang, P. To, Field observations on modal properties of two tall buildings under
 788 strong wind, Journal of Wind Engineering and Industrial Aerodynamics, 101 (2012) 12-23.
- 789 [5] F.L. Zhang, C.E. Ventura, H.B. Xiong, W.S. Lu, Y.X. Pan, J.X. Cao, Evaluation of the dynamic
 790 characteristics of a super tall building using data from ambient vibration and shake table tests by
 791 a Bayesian approach, Structural Control and Health Monitoring, 25(4) (2017) e2121.
- 792 [6] M.J. Glanville, K.C.S. Kwok, Dynamic characteristics and wind induced response of a steel frame
 793 tower, Journal of Wind Engineering and Industrial Aerodynamics, 54–55 (1995) 133-149.
- 794 [7] J.M.W. Brownjohn, E.P. Carden, C.R. Goddard, G. Oudin, Real-time performance monitoring of
 795 tuned mass damper system for a 183 m reinforced concrete chimney, Journal of Wind
 796 Engineering and Industrial Aerodynamics, 98(3) (2010) 169-179.
- 797 [8] A.P. Jeary, Damping measurements from the dynamic behaviour of several large multi-flue
 798 chimneys, Proceedings of the Institution of Civil Engineers, 57(2) (1974) 321-329.
- 799 [9] A. DeVivo, C. Brutti, J.L. Leofanti, Modal shape identification of large structure exposed to wind
 800 excitation by operational modal analysis technique, Mechanical Systems and Signal Processing,
 801 32(1-2) (2013) 195-206.
- 802 [10] J.M.W Brownjohn, A. Raby, J. Bassitt, A. Antonini, E. Hudson, P. Dobson, Experimental modal
 803 analysis of British rock lighthouses, Marine Structures, 62 (2018) 1-22.

- 804 [11]J.M.W. Brownjohn, F. Magalhaes, E. Caetano, A. Cunha, Ambient vibration re-testing and
805 operational modal analysis of the Humber Bridge, *Engineering Structures*, 32(8) (2010) 2003-
806 2018.
- 807 [12]R. Brincker, M. Lopez-Aenlle, Mode shape sensitivity of two closely spaced eigenvalues, *Journal*
808 *of Sound and Vibration*, 334 (2015) 377–387.
- 809 [13]R. Brincker, Implication of closely spaced modes in OMA, 6th International Operational Modal
810 Analysis Conference, Gijón, Spain, 2015.
- 811 [14]W. D’Ambrogio, A. Fregolent, High-order MAC for the correlation of close and multiple modes,
812 *Mechanical Systems and Signal Processing*, 17(3) (2003) 599–610.
- 813 [15]S.K. Au, Fast Bayesian ambient modal identification in the frequency domain, Part I: posterior
814 most probable value, *Mechanical Systems and Signal Processing* 26(1) (2012) 60-75.
- 815 [16]R. Brincker, C. Ventura, *Introduction to operational modal analysis*, Wiley, London, 2015.
- 816 [17]J.E. Mottershead, C. Mares, S. James, Fictitious modifications for the separation of close modes,
817 *Mechanical Systems and Signal Processing*, 16(5) (2002) 741–755.
- 818 [18]R. Pintelon, P. Guillaume, J. Schoukens, Uncertainty calculation in (operational) modal analysis.
819 *Mechanical Systems and Signal Processing*, 21 (2007) 2359-2373.
- 820 [19]E. Reynders, R. Pintelon, G. De Roeck, Uncertainty bounds on modal parameters obtained from
821 stochastic subspace identification, *Mechanical Systems and Signal Processing* 22 (2008) 948-969.
- 822 [20]M. Döhler, X.B. Lam, L. Mevel, Uncertainty quantification for modal parameters from stochastic
823 subspace identification on multi-setup measurements, *Mechanical Systems and Signal*
824 *Processing*, 36 (2013) 562–581.
- 825 [21]S.K. Au, *Operational Modal Analysis: Modelling, Inference, Uncertainty Laws*. Springer, Singapore,
826 2017.
- 827 [22]S.K. Au, Fast Bayesian ambient modal identification in the frequency domain, Part II: posterior
828 uncertainty, *Mechanical Systems and Signal Processing*, 26(1) (2012) 76-90.
- 829 [23]S.K. Au, J.M.W. Brownjohn, J.E. Mottershead, Quantifying and managing uncertainty in
830 operational modal analysis, *Mechanical Systems and Signal Processing*, 102 (2017) 139-157.
- 831 [24]Y.C. Ni, X.L. Lu, W.S. Lu, Operational modal analysis of a high-rise multi-function building with
832 dampers by a Bayesian approach, *Mechanical Systems and Signal Processing*, 86 (2017) 286-307.
- 833 [25]H.F. Lam, F.L. Zhang, Y.C. Ni, J. Hu, Operational modal identification of a boat-shaped building by
834 a Bayesian approach, *Engineering Structures*, 138(1) (2017) 381-393.
- 835 [26]H.R. Pan, Z.N. Xie, A. Xu, L. Zhang, Wind effects on Shenzhen Zhuoyue Century Center: Field
836 measurement and wind tunnel test, *The Structural Design of Tall and Special Buildings*, 26(13)
837 (2017) DOI: 10.1002/tal.1376.
- 838 [27]P. Liu, P.Y. Lian, W.G. Yang, Horizontal Resonance of a 13 Story Building Under External Machine
839 Vibrations, *Journal of Structural Stability and Dynamics*, 18(1) (2018) 1850005

- 840 [28]S.K. Au, B.B. Li, Posterior uncertainty, asymptotic law and Cramer Rao Bound, Structural Control
841 and Health Monitoring, 25(3) (2017) DOI: 10.1002/stc.2113
- 842 [29]Y.L. Tong, The Multivariate Normal Distribution, New York, Springer, 1990.
- 843 [30]R.A. Horn, C.R. Johnson, Matrix Analysis, Cambridge University Press, UK, 2013.
- 844 [31]M. Brookes, The Matrix Reference Manual, 2011. [online]
- 845 <http://www.ee.imperial.ac.uk/hp/staff/dmb/matrix/intro.html>